FM BAND CHANNEL MEASUREMENTS AND MODELLING

A THESIS SUBMITTED TO
THE GRADUATE SCHOOL OF
ENGINEERING AND NATURAL SCIENCES
OF ISTANBUL MEDIPOL UNIVERSITY
IN PARTIAL FULFILLMENT OF THE REQUIREMENTS FOR
THE DEGREE OF
MASTER OF SCIENCE
IN
ELECTRICAL, ELECTRONICS ENGINEERING AND CYBER SYSTEMS

By
Omar Mohamed Mohamed Ibrahim AHMADIN
Sept, 2018

ABSTRACT

FM BAND CHANNEL MEASUREMENTS AND MODELLING

Omar Mohamed Mohamed Ibrahim AHMADIN
M.S. in Electrical, Electronics Engineering and Cyber Systems
Advisor: Assoc. Prof. Dr. Mehmet Kemal Özdemir
Sept, 2018

As the demand for higher data rates increases every day, the need for new frequency bands becomes more and more prominent. The FM band between 88 and 108 MHz is one of the bands that are not fully utilized. This band for now is being assigned for audio broadcast around the world, however, it is expected that more people will abandon the services offered at this band. The band is characterized by great features. For instance, it retains exceptional key characteristics such as propagation, which has a large coverage range and excellent through-buildings penetration. As FM coverage is so ever-present around the world, various applications can be considered to better exploit this useful band. Thus, investigating and obtaining the key channel parameters for the FM band for the possible two-way digital wireless systems, has become of significant interest. In this thesis, we present the results of field measurements at 86 MHz conducted at Gebze, Kocaeli, Turkey. Through the measurements, some of the FM channel characteristics are identified. Measurements are performed for urban, hilly terrain, and rural areas. Our results show that the FM channel expectedly has a large coverage area but at the same time, it possesses large channel excess delays. While most of COST-207 channel power delay profile models are also applicable for the FM Band, for urban environments and hilly terrain environments, channel clusters and excess delays are also higher than those of COST-207 models. As 5G systems aim to utilize lower frequency bands for supplementary links, FM Band can be considered as one of the potential bands and the channel models proposed in this study can then be exploited for performance analysis.

Keywords: Channel Measurements, Channel Sounding, Channel Impulse Response, Power Delay Profile, Direction of Arrival, Doppler Spread, Rician K-factor, Path Loss.

ÖZET

FM BANDİ KANAL ÖLÇÜMLERI VE MODELLENMESI

Omar Mohamed Mohamed Ibrahim AHMADIN
Elektrik-Elektronik Mühendisliği ve Siber Sistemler, Yüksek Lisans
Tez Danışmanı: Assoc. Prof. Dr. Mehmet Kemal Özdemir
Eylül, 2018

Daha yüksek veri hızlarına olan talep her geçen gün arttıkça, yeni frekans bantlarına olan ihtiyaç da daha belirgin hale gelmektedir. Frekans modülasyon (FM) bandının 88 ve 108 MHz arası tam olarak kullanılmamış bantlardan biridir. Şimdilik bu bant dünya genelinde ses yayını için tahsis edilmiştir, ancak daha fazla insanın bu bantta sunulan hizmetleri terk etmesi beklenmektedir. Bu bant harika özellikler barındırmaktadır. Örneğin, bu bant geniş bir kapsama alanı ve mükemmel bina içi penetrasyonu sağlayan yayılım gibi önemli bir özelliğe sahiptir. Dünyada FM kapsama alanı her zaman mevcut olduğundan, çeşitli uygulamaların bu faydalı banttan daha iyi yararlanması gerektiği düşünülmelidir. Böylece, FM bandında olası iki yönlü dijital kablosuz sistemler için ana kanal parametrelerinin araştırılması ve elde edilmesi önemli bir hale gelmiştir. Bu tezde, biz Türkiye Kocaeli ilinin Gebze ilçesinde 86 MHzâĂŹde saha ölçüm sonuçlarını sunmaktayız. Ölçümler sayesinde, FM kanalı özelliklerinden bazıları belirlendi. Ölçümler kentsel alanlarda, engebeli arazilerde ve kırsal alanlarda yapıldı. Elde etiğimiz sonuçlar, FM kanalının geniş bir kapsama alanına sahip olduğunu ve aynı zamanda fazla kanal gecikmesine (excess delay) sahip olduğunu göstermiştir. COST-207âĂŹnin kanal gücü gecikme profili modellerinin çoğu kentsel ve engebeli arazi ortamları için geçerliyken, kanal kümeleri (clusters) ve gecikmeleri COST-207 profil modellerinden daha yüksektir. 5G sistemlerinde ek bağlantılar için düşük frekans bantlarının kullanılması amaçlandığından, FM bandı potansiyel bantlardan biri olarak düşünülebilir ve bu çalışmada önerilen kanal modelleri daha sonra performans analizi için yararlanılabilir.

Anahtar sözcükler: Kanal Ölçümleri, Kanal Sesi, Kanal Darbe Yanıtı, Güç Gecikme Profili, Varış Yönü, Doppler Yayılımı, Rician K-faktör, Yol Kaybı.

Acknowledgement

I would like to express my deep sincere gratitude to my advisor Assoc. Prof. Dr. Mehmet Kemal Özdemir for all the support he generously gave to me during the research, and for his patience and motivation. Without his patience and commitment, this work would have never been completed. I learned a lot from him, and he was a great mentor and like a father to me.

I would love to thank, the unfortunate and extremely tough life experiences that I have faced, struggled with, and suffered from so far. Frankly speaking, without them, I would not have been strong enough to face life, achieve what I have achieved, and continue in my path that far.

I also want to give a special thanks to my friends back in Egypt for their existence in my life.

Finally, I would like to take this chance to mention that without the support of my father, my mother, and my fiancee, and without their encouragement and sincere love, nothing would have had a meaning anymore at all.

Contents

List of Figures

List of Tables

Chapter 1

Introduction and Motivation

Centuries ago, non-electrical techniques were used for wireless communication to transfer the information such as smoke signals and signal flags in maritime operations. In 1830s, wired electrical telecommunication systems started to appear. While in 1870s the first electric telephone was invented, by 1878-1879 the first commercial telephone services were released [6]. Only after Alexander Graham Bell held the master patent for the telephone, all other patents for electric telephone devices were filed after this master patent. In 1882, the first telephone company, the Bell Telephone Company was established by Alexander Graham Bell and Gardiner Greene Hubbard in the United States [7]. Bell with Charles Sumner Tainter managed to do the first wireless telephone call through modulating the light-beams which is projected by photophones. In this experiment, the transmission of a wireless telephone voice message was done to Bell's laboratory window, around 213 meters away from the roof of the school. Guglielmo Marconi could be able by then to perform multiple outdoor wireless transmission experiments where the transmission distance was substantially increased. Shown in Fig. 1.0.1 is the structure of his Radio system [1].

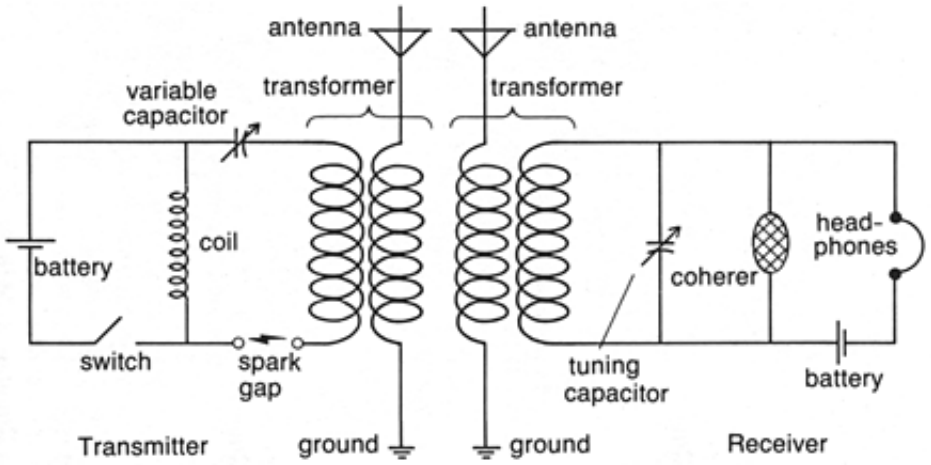

Figure 1.0.1: Marconi's Radio System [1].

Electrical wireless communication systems have been undergoing through huge enhancing developments throughout the past few decades. The starting of modern wireless communication systems started initially with the transmission of the analog voice. The first generation of wireless mobile telecommunications (1G) system was introduced in the 1980s [8]. In 1G system, voice was transmitted without any digitization, but transmitted as an analog signal. Digitizing the signal increases the system's immunity towards the noise introduced by the channel effect. Besides, there was no unified standard among all the 1G system vendors. This did not serve the compatibility of a certain manufacturer's mobile equipment with a network developed by another manufacturer. Thus, only mobile equipment belonging to the same network vendor could communicate with each other. At the end, 1G systems did not offer handover between different base stations. This did not offer the user the mobility luxury across different base stations without having the call dropped. Hence, there showed up the need to design a new unified standard that offers handover. These new systems -starting from 2G- offer the transmission of both voice and data where the digitizing of the signal took place.

Enhancements in the digital systems were focused on modifying the modulation scheme that would result into the maximum possible data rate and that would

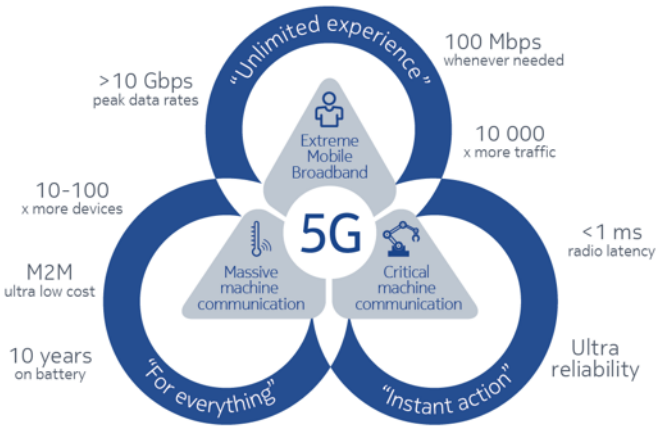

Figure 1.0.2: 5G features diagram.

best combat the undesired channel effects and noise. It should be noted that the higher the desired data rate becomes, the more distortion due to a certain channel on the transmitted signal occurs.

Starting from 2G systems till the newly developed wireless generations, the main aim was to design a system that delivers higher data rates as compared to the previous ones. Therefore, as we advance in wireless generations, the wireless channel models should be more precise and accurate about the description of the behavior of the real channel as the high data rate signals get more sensitive to the channel effects.

3G systems then set the standards for the widely used wireless technology that we have come to know. Due to the higher data rates and the wide band, 3G systems introduced video downloading, streaming, image sharing and Smartphone technology. 2 Mb/s were being handled easily in this generation [9].

For the 4G LTE, more simultaneous connections are supported on the cell. The data rates up to 100 Mb/s or to 1 Gb/s are supported [9].

For now, 5G is being tested, while the desired speed should overcome 1-10 Gb/s. On the other hand, Qualcomm offered new mmWave antennas that pave the way for first 5G smartphones. The following Fig. 1.0.2 [10] shows the main characteristics that 5G should offer.

After all, for all these wireless generation, the understanding of the wireless channel was important in developing the new systems. For this purpose, many measurements campaigns and channel modellings were carried out in order to adequately model the wireless channel behavior so that communication systems' performances are better assessed. Similarly, in this study we investigate the behavior of the FM band channel through intensive field measurements.

In general, newly developed systems deploy Multiple Input Multiple Output (MIMO) technique in the transmission of data in order to multiply the channel capacity by exploiting the multipath propagation [11]. If were to simply explain the intuition behind the concept of MIMO technique, different data signals are being sent on the same channel at the same time through different antennas. This leads to the smearing of the received signal due to the interference between the transmitted data symbols. However, multiple antennas are utilized at the receiver side as well. Each of those receiving antennas gets a different version of the smeared signal due to the variance in the channel effect on each of the transmitted data symbols. This divergence in the channel effects arises from the distinction between each path taken by each data symbol from its transmitting antenna to the multiple receiver antennas. Fig. 1.0.3 [2] below is a simple figure illustrating how the multiple receiver antennas receive different waveforms due to the multipath propagation environment.

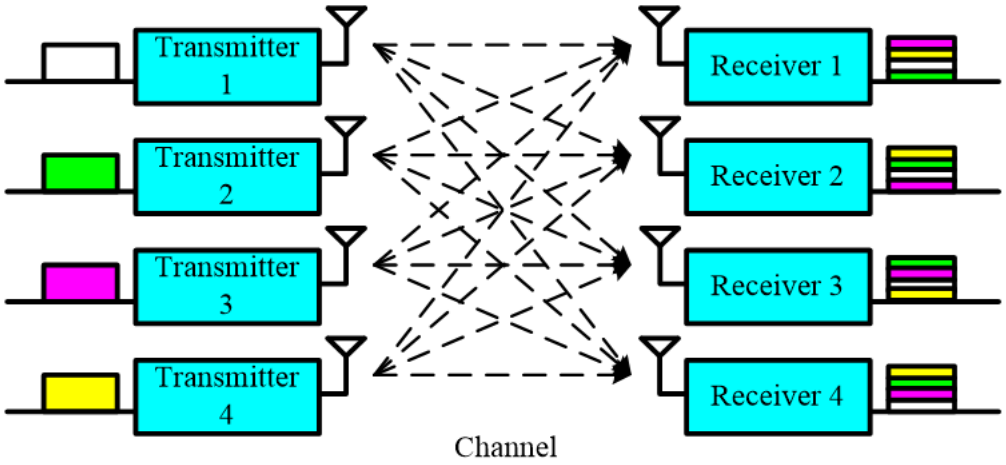

Figure 1.0.3: Illustrative figure of the MIMO concept [2].

The multiple received signals undergo complex signal processing in order to recover the original transmitted symbols. This technique as shown takes advantage of the variance in the multipath propagation of the channel through space diversity. Thus, it is important to know the direction from which different signals are received. Hence, not only a channel model, that describes the channel in terms of delay spread, rate of change of the channel effect (doppler effect) and noise, is important for the testing of the system efficiency, but also the directionality of the wireless channel must be taken into consideration for the MIMO deploying systems [11].

Due to the limited sources of the allocated known frequency bands, researchers are moving towards 5G and are aiming to achieve higher data rates through more efficient utilization of the scarce frequency bands. On the other hand, certain frequency bands are poorly utilized, such as TV broadcast bands. These bands are now being considered either for two-way digital communication or for the supplementary links of 5G downlink channels [12].

Many studies for the white space TV bands were performed. One of the earliest studies was done in 2012 at Wilmington, NC, USA as the government connected some of the city's infrastructures, provided public wireless broadband to visitors in certain areas, and remotely monitored parking lots for security [13]. This initiative happened only after the FCC approved the first device to use the TV white space spectrum in 2011, which is made by Koos Technical Services (KTS). The device is called the Agility White Space Radio (AWR) [14, 15]. In 2012, the first patent to utilize the TV white space band was filed by [16], while in 2013, the IEEE 802.11af standard for wireless communication published White-Fi [17].

On the other hand, over the time, the FM radio users are tending to move from traditional radio devices to online radio, especially the younger generation from 13 to 35 year-olds in the US [18] and the UK [19]. Moreover, between 2003 and 2013, there has been a constant gain in the profit of the online radio worldwide from 278 Million dollars to 827 Million dollars, with an annual growth average rate of 28% per year [20]. This trend indicates that the traditional analog broadcast of FM radios will phase out in the near future. Hence, a utilization

and standardization for this band is expected to happen, similar to what has happened in the analog TV band.

In this thesis, we first underlie the main parameters of a wireless channel and then we develop a measurement technique and setup for outdoor field measurements at 86 MHz. We picked the frequency to be 86 MHz because it is the band closest to the FM band since all the other FM band frequencies are occupied by the FM radio services. For this center frequency, the channel behavior is not expected to face a dramatic change from the typical FM Band channels. Moreover, we perform a wide range FM radio channel measurements that took place at Gebze, Kocaeli, Turkey. The band has good propagation properties such as higher penetration and longer range that make the band suitable for long range data communication. To the best of our knowledge, this is the first extensive attempt for the understanding of the FM channel behavior. In addition, the measurement environment was rich and of different scenarios that included: line-of-sight, non-line-of-sight, urban, hilly terrain, and rural areas. Furthermore, we process and analyze the captured data under different scenarios for different channel characteristics such as, multipath power delay profiles, Doppler spread, path loss, k-factor and direction of arrival.

The outline for the rest of the thesis is as follow: Chapter 2 explains the wireless channel behavior. Chapter 3 presents the importance of the wireless channel measurements and lays out the literature survey for the channel measurements campaigns generally carried out for different frequency bands as well as those performed specially for the FM band. Then, Chapter 4 presents the proposed hardware setup for the measurements and the equipment used therein. Chapter 5 gives the results and analysis of data captured from the measurements, while Chapter 6 concludes the work and predicts the future work.

Chapter 2

Dynamics of Wireless Channels

The incentive lying behind our work is discussed in the previous chapter, where the importance of the wireless channel modelling is demonstrated. It gave a foundation on which wireless communication systems can be evaluated. Furthermore, the behavior of the wireless channel and its effect on the transmitted signal is examined in this chapter.

2.1 Signal Transmission through Wireless Channels

It is well known that the signal propagation in the wireless channel suffers from spreading in various directions according to the radiation pattern of the antenna. The spread copies of the signal are called Multipath Components (MPCs). Each one of the MPCs tackles different scatterers and surroundings in its way to the receiver. On the other hand, some components, called Line-of-Sight (LOS) components, do not suffer from the scatterers in the channel and propagate straightly till the receiver, while the rest of the MPCs suffer from reflections due to the different Interfering Objects (IOs) in the channel environment. Such MPCs are known as Non-Line-of-Sight (NLOS) components.

In [21], it is stated that the MPCs are received in the form of clusters. For MPCs group that leave the transmitted antenna within a very small range of departure angles and arrive within a small range of arrival angle at the receiver, It is called a cluster. Accordingly, the received signal in the multipath wireless channel arrives as a number of received clusters, each of which has a unique delay spread, Angle-of-Departure (AOD) and Angle-of-Arrival (AOA) as shown in Fig. 2.1.1 [22]. The figure shows that the receiver receives 3 clusters, each of which consists of several MPCs. For a better demonstration, it can be shown that each large arrow, or cluster, is composed of smaller arrows representing MPCs. 3 variables define an MPC: its Direction of Departure (DoD), Direction of Arrival (DoA), and its Time of Arrival (ToA). A main MPC is present in every cluster, and the arrival time and directionality of the cluster only refer to the properties of the main MPC. The first MPC received from a certain cluster is typically considered to be the main MPC.

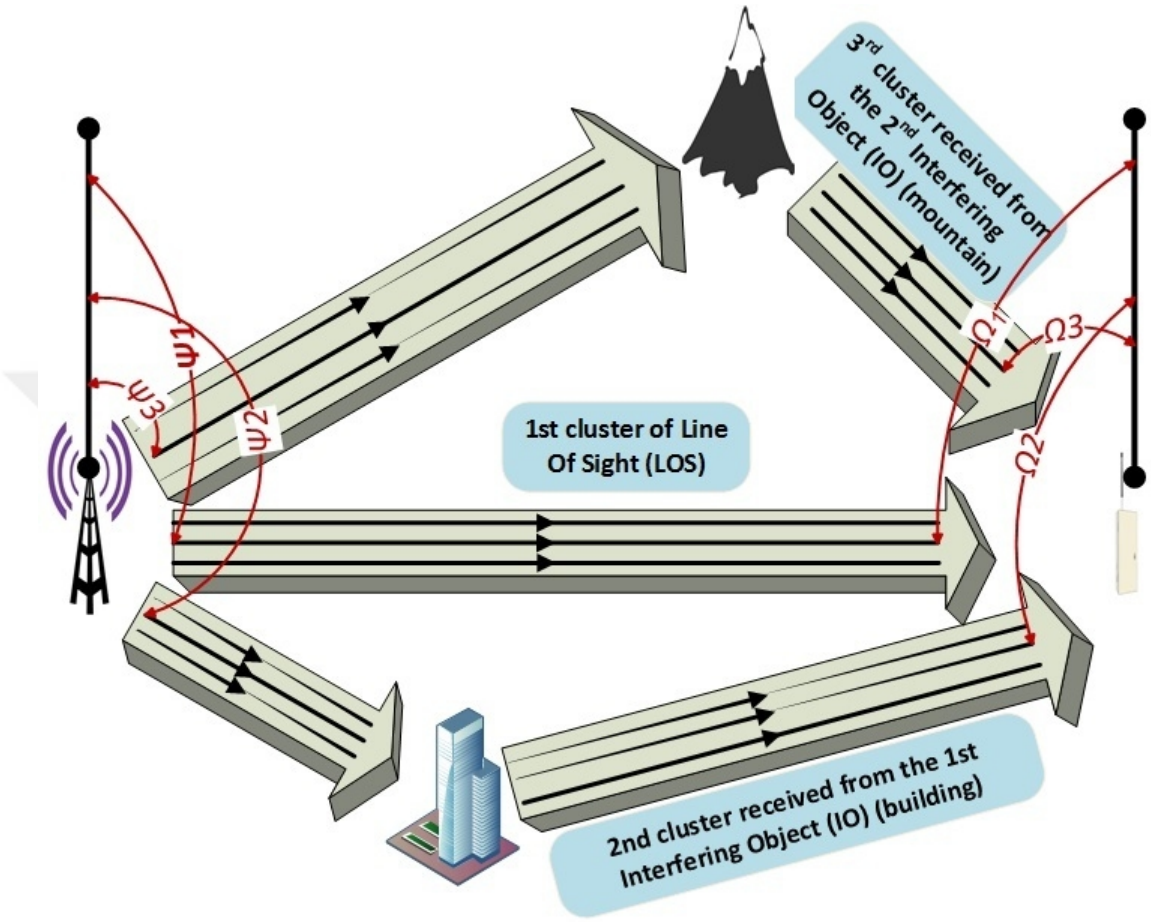

Figure 2.1.1: Illustrative Figure of clusters concept.

The channel delay spread is constrained by two aspects: the time at which each cluster begins and the delay spread within each of those clusters. The intensity of the signal received through a multipath channel as a function of time, is known as the Power Delay Profile (PDP). Additionally, the difference in the travel between multipaths arrivals is defined as the time delay. Since the PDP does not include the delay between the transmitter and the receiver, on the PDP graph; the first received MPCs starts at time zero.

The reception of many clusters is shown in Fig. 2.1.2 [3], where a noticeable general exponential decay with the increasing of time occurs. This is typically the general case for indoor and outdoor environments as mentioned in many studies [21, 23, 24]. The PDP shown is possible for an indoor environment with a high

frequency of operation, although it is also applicable for outdoor environments.

This is expected considering the delay spread is too small (in nanoseconds). In the case of indoor environments IOs are usually in the vicinity of the receiver. Hence, high frequencies suffer large attenuation. Thus, it is unlikely that the cluster can survive to a remote IO and reflect back to the receiver non-attenuated.

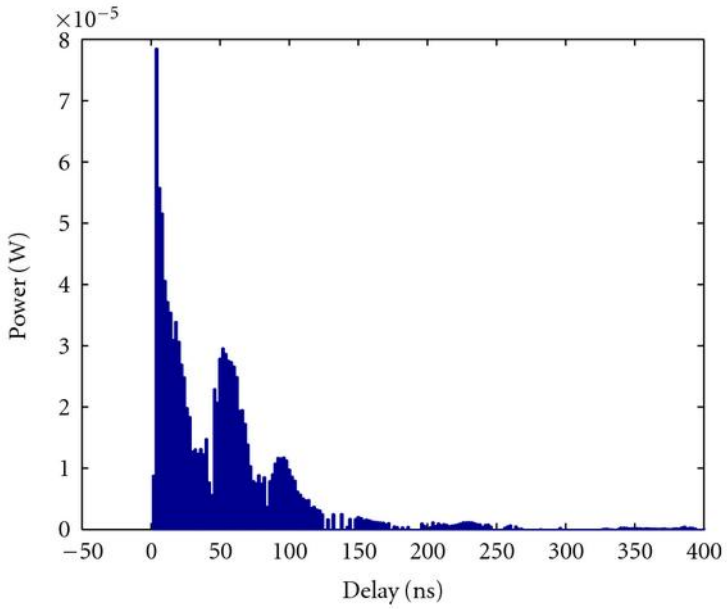

Figure 2.1.2: Illustrative figure showing the exponential power decay within each cluster with the advance of time. [3]

In digital communications, there is a need to discretize the channel into N taps or distinct bins. Within a bin, MPCs received are unresolvable by the receiver and interpreted as a single tap. The bandwidth of the signal defines the maximum possible sampling period of the channel. There is an inversely proportional relationship between the signal bandwidth and the maximum allowed sampling period. It can be physically explained as follows: an increase in the signal bandwidth is accompanied with a decrease in the symbol duration. This causes the signal to be more sensitive to the time distortion. This distortion is usually caused by the arrival of the late MPCs or the echoes of the signal due to multipaths, which might introduce Inter-Symbol Interference (ISI). Thus, for a

better channel modelling, higher sampling rate is required in order to take into consideration more channel effects by reducing the sampling period.

Since the number of the received MPCs is typically very large, and in order to determine how the PDP will look like, the bandwidth of the system has to be taken into consideration. For instance, when the system bandwidth is too large, small sampling period becomes essential. In this case, the channel may look continuous since large number of MPCs are received within a short interval with a high resolution. The PDP shown below in Fig. 2.1.2 is a possible case. On the other hand, for a system with smaller bandwidths, such high resolution becomes unnecessary and therefore, more MPCs arriving within the longer sampling period are represented by a single tap. As a conclusion, the more the bandwidth of the signal becomes, the more the PDP of a certain channel appears to become continuous due to to the increase in the number of resolvable taps.

Fig. 2.1.3 [22] shows a discretized PDP This way of discretization becomes very useful when the channel effects are introduced to the signal in computer modelling. There, the signal is discretized and the channel effect is introduced to the signal in simulations with the help of discrete signal processing techniques.

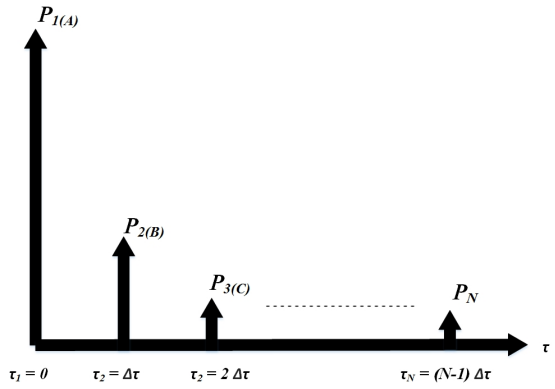

Figure 2.1.3: PDP of an N tap channel with equal spacing of $\Delta\tau$.

Note that ISI becomes very significant when the time distortion is too large. Small time distortion may just lead to the addition of different copies of the same symbol with each other. These copies may add constructively or destructively

when there is a phase difference. When the delay spread is large as compared to symbol duration, copies of different symbols will start interfering with each other. To overcome this effect complex equalization techniques need to be developed at the receiver side to remove the ISI effect. However, first of all, the ISI effect has to be accurately modelled in order to be able to remove that effect. Fig. 2.1.4 shows the overlap that happens in time domain between different copies of different symbols where A, B and C are three different channel taps [4].

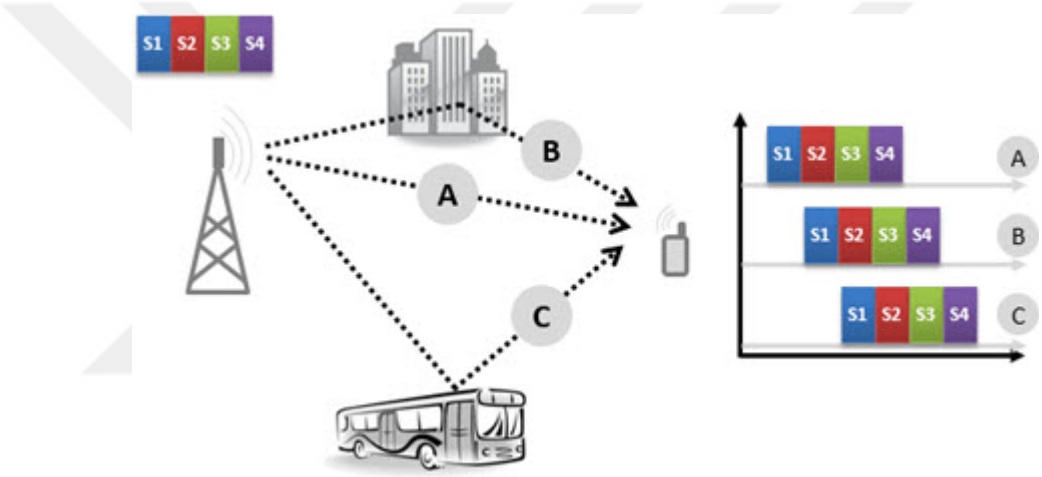

Figure 2.1.4: Illustrative figure of ISI effect [4], where A, B and C represent a 3-taps channel as indicated in Fig. 2.1.3.

2.1.1 Mathematical Channel Model

According to the previous explanation and regardless of the clusters concept, an N-tap channel can be represented by

$$h(t,\tau) = \sum_{n=1}^{N} c(t)\delta(\tau - \tau_n) \tag{2.1}$$

where $h(t,\tau)$ is the Channel Impulse Response (CIR) that describes the behavior of a certain channel when a unit impulse is being sent, $c(t)$ is the complex amplitude of the n^{th} tap, δ is the Kronecker delta function and τ_n is the time at which the n^{th} tap gets received as compared to the first tap that is assumed to be received at zero.

The delay spread of the channel is considered to be a measure for the channel selectivity in the frequency domain. The signal is convolved with the CIR in the time domain that corresponds to a multiplication in the frequency domain. For a single-tap channel, the frequency response of the channel $H(f)$ is constant for all frequencies f. Therefore, for such a case the channel is considered to be flat for all the frequencies of the signal where it affects all the frequency components of the signal with the same amplitude. However, wireless channels are not single-tap channels typically. As the delay spread of the channel increases the channel becomes more selective, affecting different frequency contents of the signal with different amplitudes. This selectivity requires equalization of the channel at the receiver.

The bigger the delay spread gets, the more complex the equalization process becomes. The coherence bandwidth is defined as the bandwidth through which the channel is considered to be flat. Thus, the coherence bandwidth of the channel decreases with the increase of the delay spread. In order to make good equalization at the receiver, a good channel estimate should be done where the delay spread of the channel has to be well modelled. This is one of the points that shows the significance having a good channel model [25, 26, 27, 28].

2.1.2 Doppler Effect in Wireless Channels

The PDP is typically derived by averaging the received power over a local area. This PDP is then sampled into N taps and the channel delay spread is calculated through the PDP. Within that local area, the CIR changes from one position to another. This change is only in the form of a change of the complex amplitudes of the channel taps $c(t)$, not in the form of an increase or decrease in the number of taps itself. This comes from the assumption that the channel does not change dramatically within a small local area. To sum it up, within a local area, according to the long term statistics, the PDP is constant and so is the corresponding delay spread while the CIRs differ from one location to another by the change in the complex amplitude of the fixed channel taps. Hence, $c(t)$, is the only function of

time t in the equation as shown.

This change with time is due to the motion of the transmitter, receiver or one or more of the surrounding IOs. This motion results into the change of the CIR within the local area. Therefore, the complex amplitudes of the channel taps change with time. The amplitude of the channel taps within a local area is agreed widely to be Rayleigh distributed for the NLOS channel taps and Ricean distributed for the LOS channel tap [23, 25]. This effect of change in the CIR with time is known as the Doppler effect. In the frequency domain, a frequency shift occurs for the received signal. This shift is positive if the receiver is moving towards the transmitted signal and negative if it is moving away from it [29]. Moreover, it is important to mention the relation between the Doppler spread and the coherence time.

Note that the receiver might be still in its position while the CIR changes due to the motion of the transmitter and/or the surrounding IOs. Therefore, the change of the complex amplitude of a certain tap in the CIR is related to the "relative" velocity of the receiver with respect to the direction from which that tap is received [25, 27].

In order to study the Doppler effect from another perspective, let's consider it in terms of frequency domain. In frequency domain, the Doppler spread refers to the frequency shift that happens to the received signal where some frequency bands might be received at the receiver side without originally being transmitted at the transmitter side. That is, the receiver is receiving some data that had not been part of the sent signal. Fig. 2.1.5 [5] simply shows that the receiver whose direction of motion is against the direction of arrival of the signal (the one on the right) is actually receiving the signal with a frequency higher than the original one. The receiver on the left is in contrast with that case.

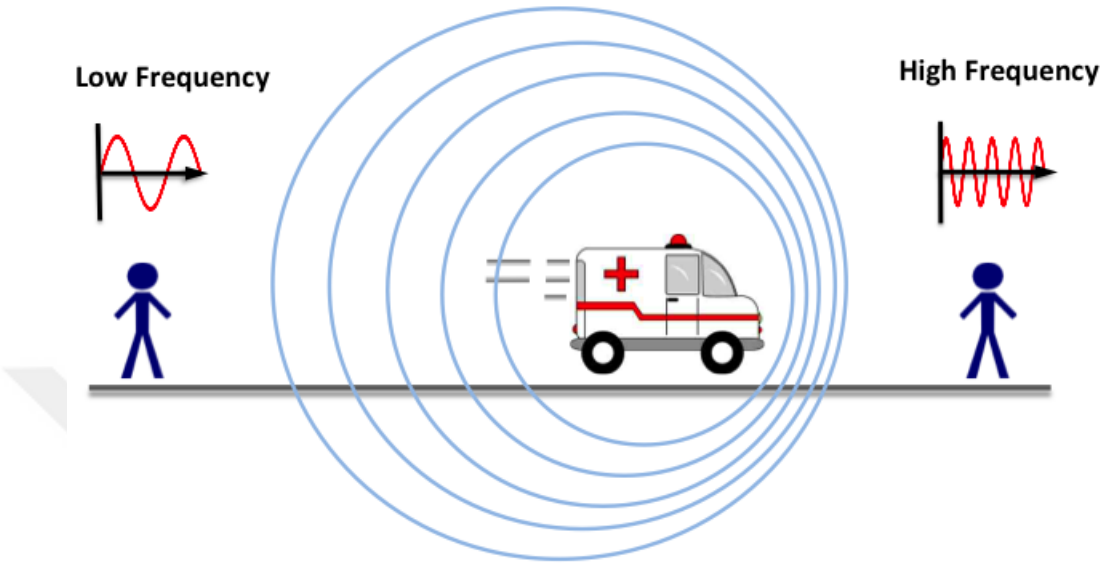

Figure 2.1.5: Frequency shift of the received signal due to the relative velocity of the receiver with respect to the direction of arrival of the signal [5].

If a tap is received from a direction perpendicular to the relative velocity of the receiver, there will be no frequency shift, meaning as if there is no motion at all. The received frequency will be the same as the transmitted one then. Thus, the Doppler spectrum varies with the movement scenario in the environment where each channel delay tap may have its own unique Doppler spread depending on the direction of movement of the receiver with respect to the direction from which the tap is received.

Generally, it is intuitional to expect a relatively fast change in the CIR when the relative velocity of the receiver is high, while the change in the CIR is slower when the velocity is less. As discussed in [25], the channel coherence time is an indication of the time varying nature of the channel. It is the time over which the CIR is invariant. The coherence time T_c is calculated as the inverse of the Doppler spread as $T_c = 0.423/f_m$, where f_m is the maximum Doppler shift given by $f_m = v/\lambda$.

In a design of a system, it is important to have the duration of any transmitted symbol to be less than the coherence time of the channel. Achieving this condition

makes the compensation of the channel effect during a single symbol a simpler process since the channel is considered to be constant along the whole symbol duration. The receiver makes a channel estimation as a first step in order to be able to equalize the received signal. Since the symbol duration is shorter than the coherence time of the channel, the channel estimate that the receiver has is not expected to change dramatically along the whole symbol duration and therefore, this single estimate is sufficient to make a good equalization while no other estimate needs to be done within the same symbol. Other channel estimates might be needed after the coherence time of the channel. This is another point showing the importance of having a good channel model so that the system design suits the given channel conditions. The coherence time shall be well modelled and accordingly the symbol duration should be determined. Therefore, in order to know the time in which the channel is almost invariant it is of an importance to measure the Doppler spread for a better understanding to the channel behavior.

In this thesis, we present the results for our measurements campaign for the key aspects of the FM channel band. Those key parameters for the channel include: CIRs, DoAs, Doppler spreads, PDPs, Coherence Times and K-Factors. Those parameters are obtained for each receiver location.

2.2 Chapter Conclusion

This chapter explained the basic concepts that shall be adopted for the understanding of the wireless channel effect on the transmitted signal. It also illuminated the importance of having a good channel model for the purpose of designing a communication system that performs well in a given channel. Thus, channels have to be accurately described by the model to result into a good performing system and to successfully assess the performance.

Chapter 3

Outdoor Measurements in a Nutshell

The behavior of the wireless channel and its effect on the transmitted signal is examined in the previous chapter. Some of the channel parameters has been discussed with mentioning of the importance of obtaining those parameters. In this chapter a brief literature survey is carried out for the wireless communication measurements with a focus on the FM band.

It is important that the behavior of a wireless channel has to be determined in order to utilize it. This behavior at a certain frequency can be known accurately via real measurements in different types of environments whether indoor or outdoor environments. As a result, channel measurements are indispensable for designing any wireless system, since the wireless channel is the only factor that determines the ultimate performance limits of any communication system. At the very beginning of cellular communications systems, what has been the key role were both fading and path loss of the narrowband channel. Moving towards MIMO, wideband, and multiusers systems, new radio channel features come into account such as, directivity and frequency selectivity.

Over decades, the behavior of wireless channels are being studied and standardized in order to better analyze various wireless systems. Wireless channel behavior at a certain frequency band can be better understood via real measurements in different types of environments of indoor or outdoor. Once the behavior of the wireless channel is determined, it can then be described statistically like the famous Saleh and Valenzuela model [21]. The statistical model may have some adaptive parameters so that a wider range of wireless channels are supported, i.e., different frequencies or different environment types.

Statistical methods are the simplest approach for modelling the wireless channels and it proved its reliability over alternative methods [30]. This approach was used successfully for many frequency bands, but, to the best of our knowledge, none of these approaches used for the FM band. FM band usually left non touched as it thought to be only for analog voice broadcasting services. As a result, FM band between 88 and 108 MHz is one of the bands that are not fully utilized. This band for now is being assigned for audio broadcast around the world. The band is characterized by great features. For instance, it retains exceptional key characteristics such as propagation, which has a large coverage range and excellent through-buildings penetration.

It is of importance to mention that for the previous FM band channel measurements, only path loss is carried out for hilly and forested terrain [31, 32], while it does not provide the key aspects of wireless channels, such as the directionality and the multipath profile, it does not reveal critical channel parameters needed for digital communications. Clearly, it is incomplete model to be used for wireless systems. Moreover, for a hilly terrain channel at 145 MHz, measurements has been carried out to investigate the multipath behavior of the channel that is suitable for single-antenna transceivers [33, 34].

On the other hand, for other bands, various measurements have been performed for different channel scenarios for the multipath measurements. For example, for a hilly region, the multipath delay spread has been measured at 210 MHz [35], while multipath propagation measurements has been carried out in UHF band at 900 MHz in [36] which focused on obtaining the worst-case profiles

for typical operating locations. As for 5G, measurements using M-Sequences with USRPs are done in [37] for an extreme industrial environment.

For directionality, a vast variety systems for the Direction of Arrival (DoA) estimation are proposed in literature. Many methods were based on the Angle of Arrival (AoA), the Time of Arrival (ToA), the Time Difference of Arrival (TDoA), and beam-forming while taking into account the antenna arrays are discussed in details and comparative analysis in [38, 39, 40, 41]. As for the antenna switched measurement system that we use in our measurement system as discussed in 4, a similar study used 32 dual-polarized elements for real time 3-D dual-polarized measurements based on an antenna switched system in [42]. Moreover, in a single receiving channel with a single transmitter and M receiving antennas, a switch antenna array system is introduced to localize multiple narrowband targets using RADAR [43]. A system inspired by the human ear introduced a DoA technique using two-antenna is discussed in [44]. Lately, a similar study to ours, which used switched-antenna system to obtain the direction of arrival (DoA) proposed a measurement technique for the DoA using two-antenna single RF front end DoA estimation by obtaining and processing the I/Q data from the spectrum analyzer [45].

Hence, as FM coverage is so ubiquitous around the world, several applications can be considered to better exploit this useful band and since the multipath and directionality did not grasp much attention for the previously mentioned reasons, it is of significant interest to investigate and characterize the full channel properties of the FM Band for the potential wireless systems including the multipath power delay profiles (PDPs), DoA, and Doppler spread.

Chapter 4

Outdoor Measurement Setup

In this chapter, we will introduce the proposed measurement setup used for our measurements. It is well known that the most basic measurement setup for wireless communication channel consists of a transmitter (Tx), a wireless channel, and a receiver (Rx).

The setup that we have developed for outdoor measurement provides reliable measurements for both cases of DoA and multipath measurements. We will describe our Tx-Rx devices, antennas, cables, RF switches, the controller, GPS clock antenna, as well as, software programs for capturing data, and other tools that are related to our procedure for measurements.

4.1 Overall Diagram

The overall measurement setup for DoA measurements is presented in Fig. 4.1.1. In this setup we used a switched linear antenna array at the receiving end using RF switches with a micro-controller, while for the case of multipath and Doppler measurements, we used a single receiving antenna. This setup is shown in Fig. 4.1.2.

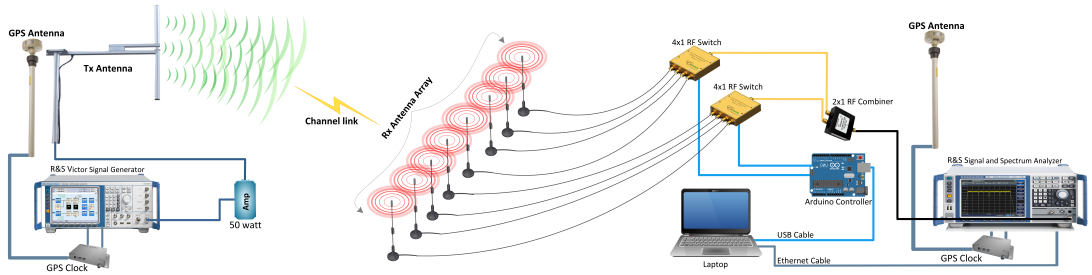

Figure 4.1.1: Overall Communication System (Antenna Array For DoA)

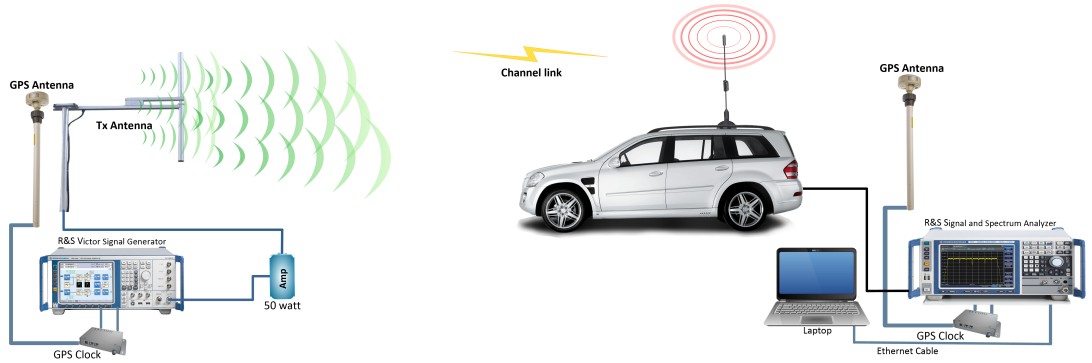

Figure 4.1.2: Overall Communication System (Single Antenna)

4.2 Measurement Equipment

4.2.1 Transmitter and Receiver

Our transmitter is a R&S SMBV100A Victor Signal Generator. It is used for transmitting a designed pulse signal with a certain power level and a specific center frequency. At the receiver side, we have a R&S FSV Signal and Spectrum Analyzer, which receives those pulses in a form of I&Q. Both devices are shown in Fig. 4.2.1

(a) R&S Victor Signal Generator(Tx)

(b) R&S FSV Spectrum Analyzer(Rx)

Figure 4.2.1: Transmitter and Receiver

4.2.2 Transmitter and Receiver Antennas

The transmitter was on top of the Electrical Engineering building, which has a height of 15 m and the receiver was put in a Sport Utility Vehicle (SUV), whose height is approximately 2 m.

Our transmitter antenna is an omni-directional FM dipole antenna with 2.15 dBi gain and wide range, while our receiver antenna is an outdoor telescopic FM antenna with 3 dBi gain. Both of them are shown in Fig. 4.2.2

(a) Tx Antenna (b) Rx Antenna

Figure 4.2.2: Transmitter and Receiver Antennas

Figure 4.2.3: Mini-Circuits Amplifier

4.2.3 Amplifier

We used Mini-Circuits LZY-1 amplifier, which is an Ultra-Linear RF amplifier with an output up to 50 Watts for the frequency range of $20 - 512$ MHz. The amplifier was hit with 0 dBm so that the antenna input power is 44 dBm. The amplifier is shown in the following Fig. 4.2.3.

4.2.4 RF Switches/Combiners

For DoA, we used a switching antenna system in order to capture the readings from each antenna independently. Thus, RF switches are required. We used two 4x1 switches (Mini-Circuits switch ZSWA-4-30DR) with a direct contact to the 8 Rx antennas, and a 2x1 splitter/combiner (Analog Devices switch HMC574AMS8E) switch to combine the input from each 4x1 switches. After combining the two switches, the cable goes directly to our R&S FSV Signal and Spectrum Analyzer. RF 4x1 switch and 2x1 splitter/combiner are shown in Fig. 4.2.4

(a) 4x1 RF Switch (b) 2x1 Splitter/Combiner

Figure 4.2.4: RF Switches

4.3 Measurement Softwares

4.3.1 Tx Software

In order to design a suitable signal for transmitting and loading it to the R&S SMBV100A Victor Signal Generator, a R&S ARB Toolbox software is used. Through this program we can design a pulse as the following Fig. 4.3.1 After designing the pulse we upload it to through the device's IP address.

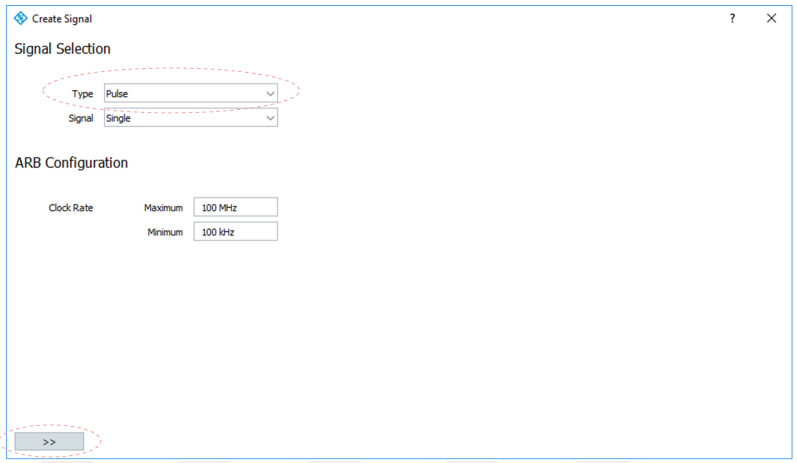

Figure 4.3.1: ARB toolbox pulse design

4.3.2 GPS: Clock, Antenna and Software

Figure 4.3.2: GPS Antenna

For the sake of synchronization between our Tx and Rx, we can use cables between Tx and Rx. This is a good solution for indoor measurements, but in our case for outdoor we need a GPS clock to handle this synchronization. The GPS antenna is shown in Fig. 4.3.2. The used clock is EPSILON CLOCK (MODEL EC1S) made by SPECTRACOM. A highly stable and accurate frequency is generated and disciplined using GPS input. The main feature for the clock is to maintain and generate the following:

- Time reference which is synchronized. 1PPS signal is also generated.
- Reference frequency (sine wave) at 10 MHz.

To make sure that our GPS clock is triggered and active, a software called Epsilon is used. Through this software, we see the status of the clock and antennas, whether they are connected or not, and how many satellites links are available. A screenshot during the measurements for the program in case of connected status is shown in Fig. 4.3.3

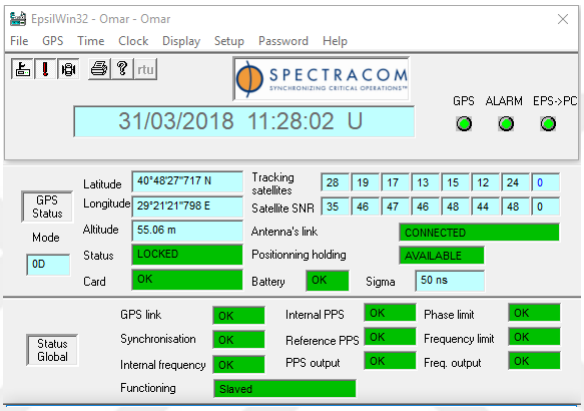

Figure 4.3.3: Epsilon

4.3.3 Rx Software

In order to capture the signal from the R&S FSV Signal and Spectrum Analyzer and convert it to ".mat" file, the R&S IQ wizard software is required. In this software we define the IP address for the FSV, the number of samples we want to capture, and the sampling rate. IQ Wizard interface is shown in Fig. 4.3.4

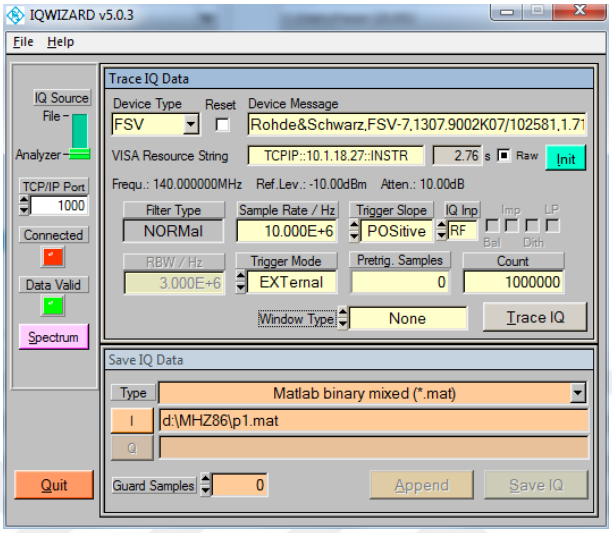

Figure 4.3.4: IQ Wizard

4.4 Measurement Place

Our measurements took place at Gebze, Turkey with different sites. With a SUV carrying the receiver set and a fixed transmitter on top of a building at Gebze Technical University, we were able to roam over different environments and scenarios for various channels. For stationary measurements, we stopped and captured our data points at each measurement location, besides storing the GPS locations using Google maps application, while for high speed measurements we took measurements continuously. The measurement points for one of the measurement sites is given in Fig. 4.4.1 for the $5Km$ short range field, while for $9.5Km$ long range field measurements it is shown in Fig. 4.4.2.

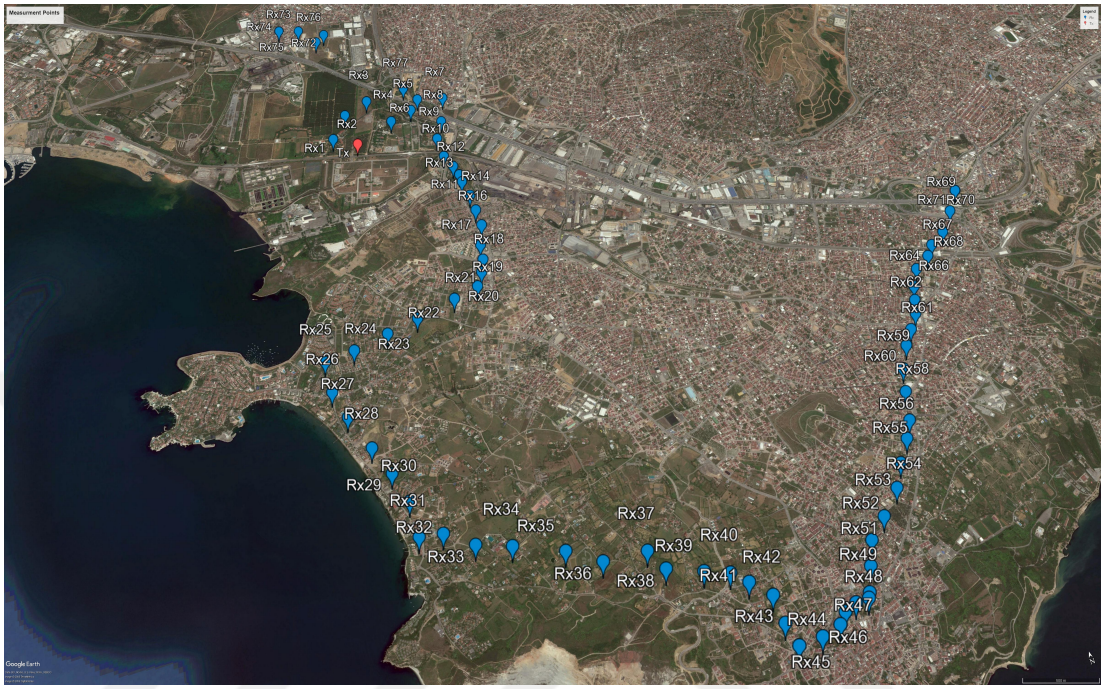

Figure 4.4.1: Measurement Points Allocated On The MAP: Blue points are the receiver points, while the transmitter is in red.

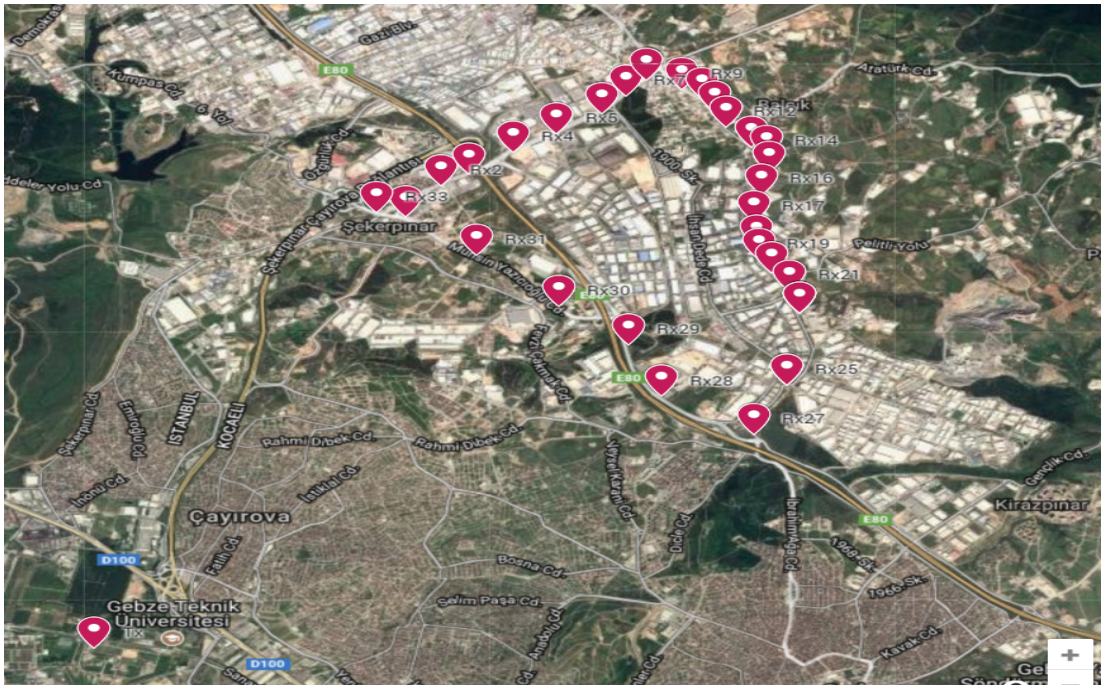

Figure 4.4.2: Measurement Points Allocated On The MAP For The Far Field.

For the current thesis, measurement results from the campaigns that are carried out during sunny days of April 2018 are presented.

4.5 Setup Functionality Validation

In this section we will test our methodology in detail. First, we will make a test to make sure that our devices and software are functional using a direct cable to cable communication link without antennas and with a delayer. For this scenario, the synchronization between the transmitter and the receiver is established via direct cable connections.

Secondly, we will perform a test with antennas to make sure that our antenna array switching technique for DoA is ready to be used in outdoor field out of the campus. First test was done indoor, while the DoA tests is done outdoor inside Gebze Technical University campus.

4.5.1 Multipath Test

4.5.1.1 Connections:

In Fig. 4.5.1, the connection between Tx and Rx is shown.

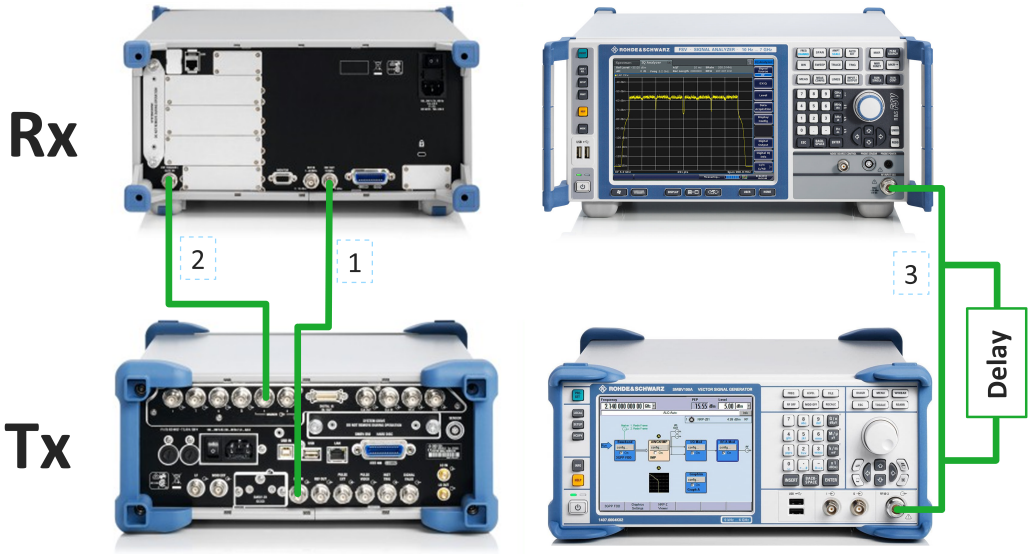

Figure 4.5.1: Connection between Tx and Rx

Below are the steps for connections:

1. Connect the RF input of the Tx with the RF output of the Rx.
2. Connect the marker of the Tx with the external trigger of the Rx. (Note that: we do this only in case of an indoor measurement within short distances between Tx and Rx. Otherwise, we unplug this and use a GPS clock instead for synchronization.)
3. Connect two RF cables; One of which represents a direct LOS path and the other represents the delayed path. The delay is represented by a SAW filter with a time delay of 4.21 μs which operates at 140 MHz.

4.5.1.2 Steps for measurement procedure:

1. **Designing The Transmitted Signal:**
   We open the R&S ARB Toolbox PLUS V 2.4 program on our PC that is connected on the same network and we follow the below steps:

- As shown in Fig. 4.5.2. Go to file menu and select create. We see the following figure: We can select any kind of waveform. In this test we select a pulse and then click next.

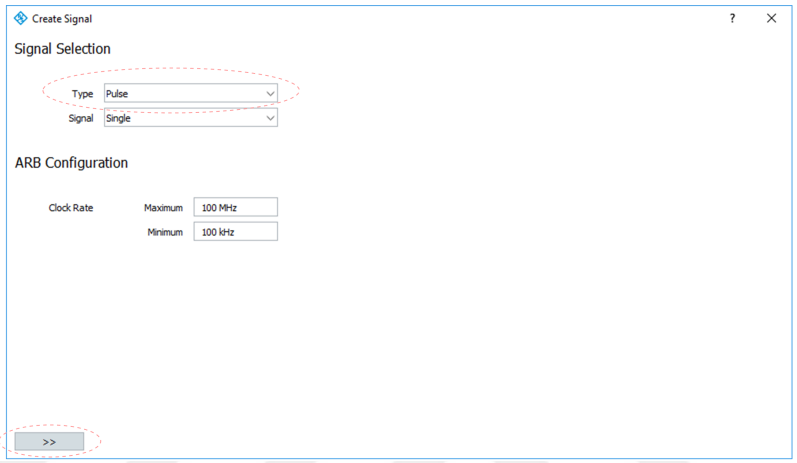

Figure 4.5.2: ARB toolbox: Pulse Design (1)

- As shown in Fig. 4.5.3. We write our pulse settings and select next:

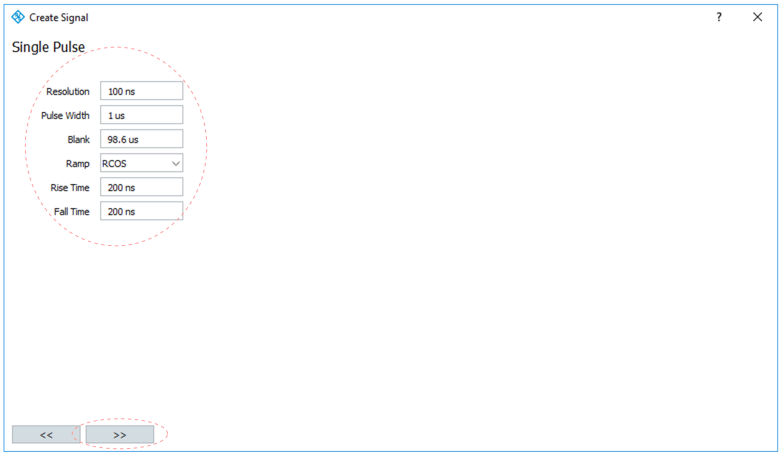

Figure 4.5.3: ARB toolbox: Pulse Design (2)

Where:

Time Resolution: *The sampling time. Every sample = 100 ns.*

ON Time: *The pulse width.*

Blank Time: *The pulse period duration.*

The full duration is: $200ns + 1\mu s + 200ns + 98.6\mu s = 100\mu s$.

- As shown in Fig. 4.5.4. We select force zero peak, and we keep number of samples in our mind. Then we select next:

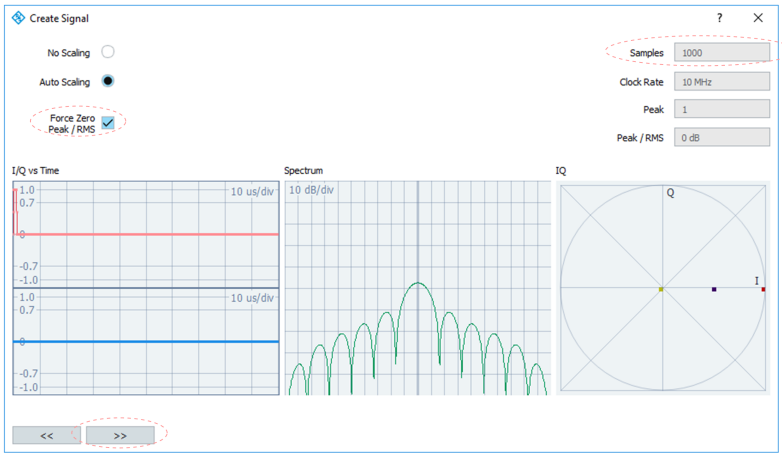

Figure 4.5.4: ARB toolbox: Pulse Design (3)

- We save our wave(1usPulse_100usDuration.wv) file in a certain destination and select Run as shown in Fig. 4.5.5:

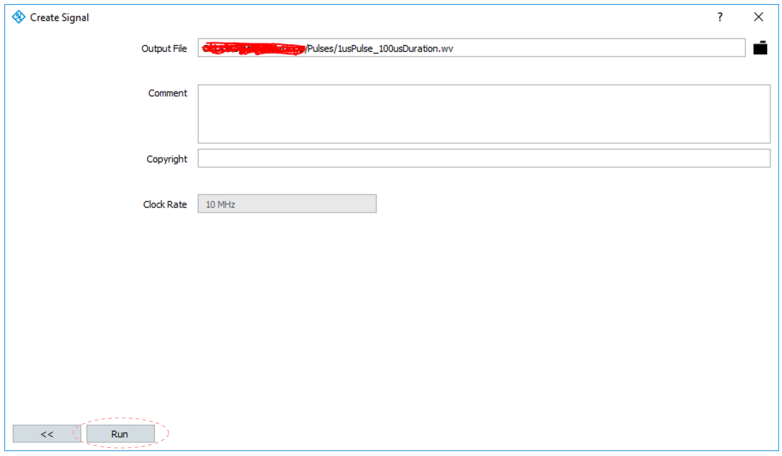

Figure 4.5.5: ARB toolbox: Pulse Design (4)

- Now we have created a waveform. We put a marker on the rising edge to be detected by the Rx. First, we go to our file that we have just saved and select it by clicking on it one right click. Then from the *Edit* menu we select *Markers* as shown in Fig. 4.5.6

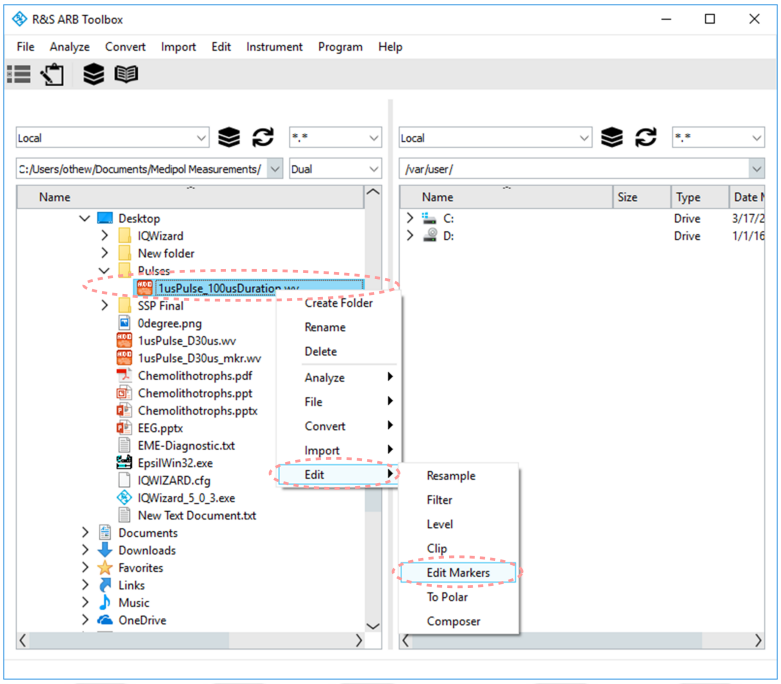

Figure 4.5.6: ARB toolbox: Pulse Design (5)

- We write down any point before the rising edge time on the cursor to make the marker be detected before the rising edge as the following and then select Run as shown in Fig. 4.5.7

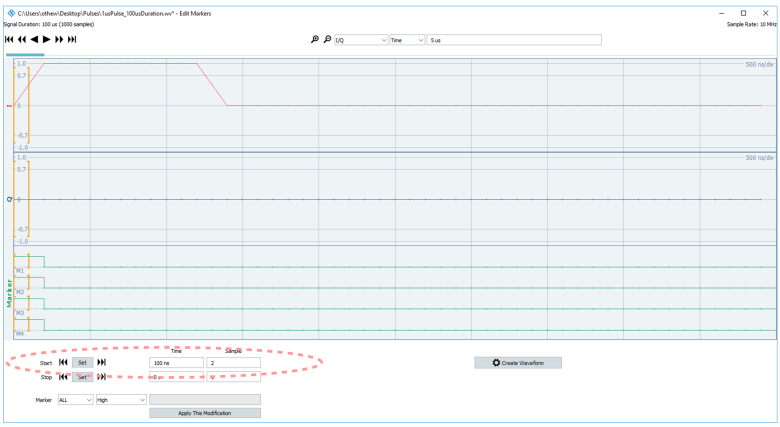

Figure 4.5.7: ARB toolbox: Pulse Design (6)

- Once we select Run, we notice a new file has been created under the same name with additional "mkr" as (1usPulse_100usDuration_mkr.wv) as shown in Fig. 4.5.8

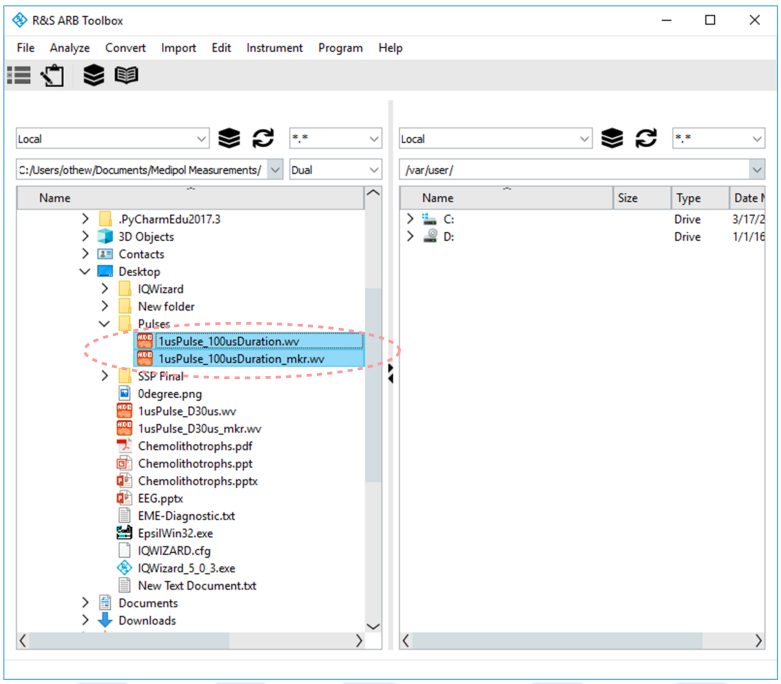

Figure 4.5.8: ARB toolbox: Pulse Design (7)

2. **Uploading The Signal To VSG (Tx)**

We open the R&SÂőARB Toolbox PLUS V 2.4 program on our PC that is connected on the same network as the following Fig. 4.5.9and follow the following steps:

- Once we open it, we select this colored icon on the right.
- When the left window appears, we select add and go to our Tx settings to know the IP address assigned for it. Then write it down.
- We go to local menu on the right and select our Tx.
- Now we drag the new signal file from Fig. 4.5.8, and drop it into the right window that is assigned for our Tx.
- We disconnect Tx from the ARB tool box program in our PC.
- This is shown in the following figure:

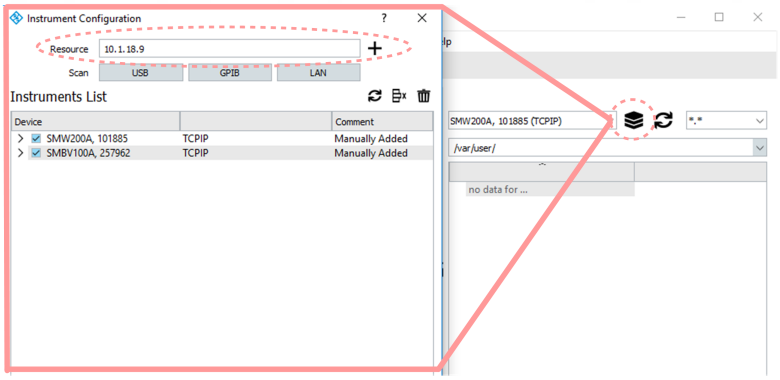

Figure 4.5.9: ARB toolbox: Pulse Design (8)

In order to adapt our frequency, power level and load the wave file. We look at the screen of the VSG which is shown in Fig. 4.5.10 and follow the following steps:

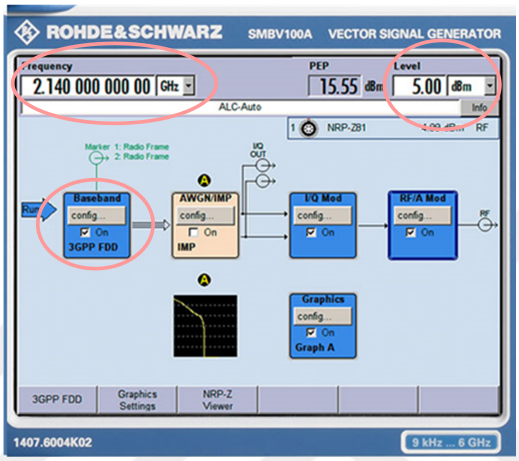

Figure 4.5.10: VSG Parameter Tuning

- We select Baseband configurations > ARB > Marker > Select 1us-Pulse_100usDuration_mkr.wv.
- We select also our frequency and our power level. In this test we select a $140MHz$ and $-20dBm$.
- We used $140MHz$ because it is the SAW filter operation frequency as this sub-assembly is available in our lab. This setup is used to validate the setup.

3. **Capturing The Received Signal**

In order to capture the received signal in MATLAB format for processing and analyzing, we use the R&S IQ Wizard software as shown in Fig. 4.5.11 as following:

- We Change the following values:
  - Select Device Type: FSV.
  - Write down in the VISA Recourse String the IP address for Rx. (Edit only the numbers and leave the TCPIP:: and ::INSTR alone)

- Select our sampling rate (It should be the inverse of our Resolution Time).
- Trigger Mode: External.
- Count: $1x10^6$.
- Type: Matlab binary mixed.
- The name of the file is p1.mat.
- Select Trace IQ and save the file.

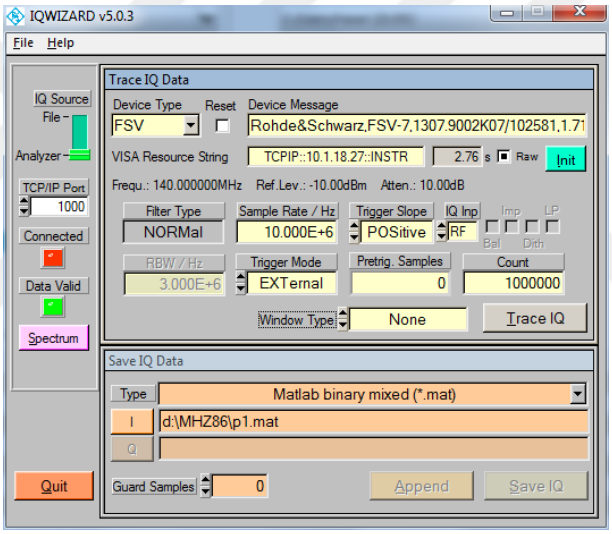

Figure 4.5.11: IQWizard Parameter Tuning

- Now we have sent from the Tx 1000 continuous samples and the Rx received $1x10^6$ samples. Everything now is saved in the p1.mat file. Redo again for p2.mat and p3.mat.
- We put those p1.mat, p2.mat, and p3.mat in the same folder with the ChannelImpulseResponse.m file, which has our code to obtain the channel impulse response.
- We run the ChannelImpulseResponse.m, and note that:
  - The parameters in the beginning of the code changes with the changing of the number of samples, frequency, and sampling frequency.
  - We have to multiply the time axis with the resolution time.

- The final results are shown in the following Fig. 4.5.12 and Fig. 4.5.13:

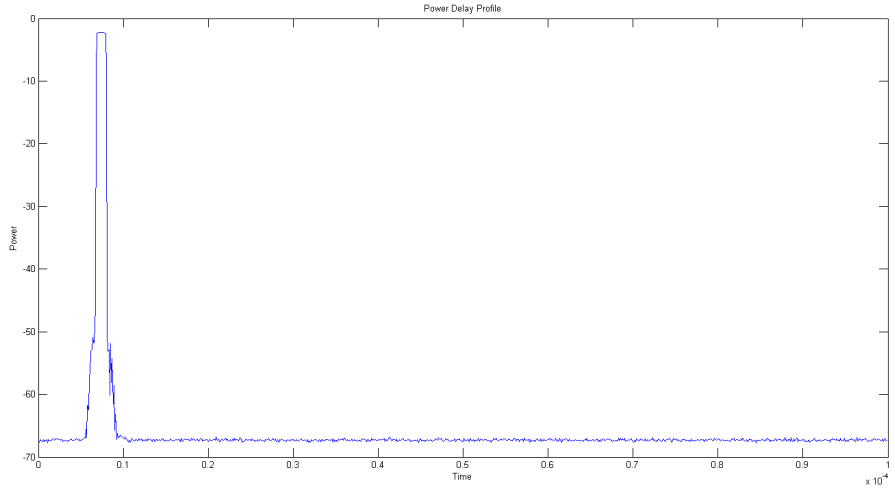

Figure 4.5.12: Transmitted Signal

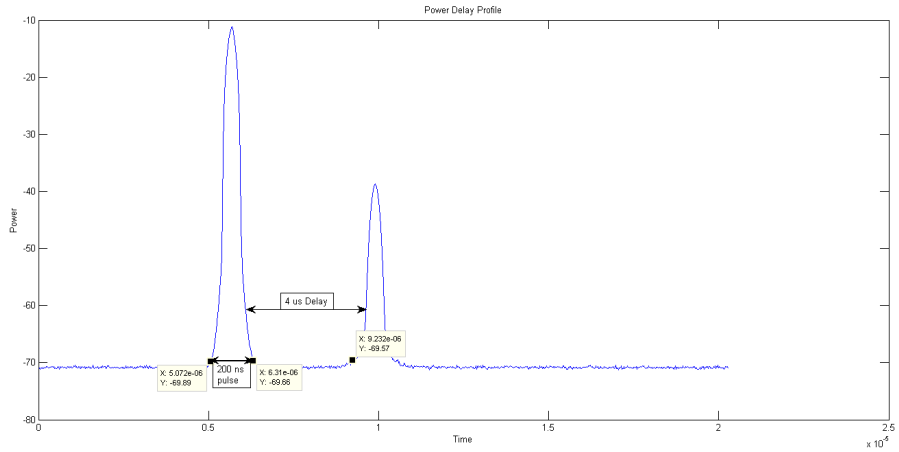

Figure 4.5.13: Received Signal

- This final result is for an 4 μs delay sub-assembly. Notice that the power is attenuated due to the RF components.
- As we expected to see at the final graph two paths, one is from the direct path and one from the delayed path.

4.5.2 Directionality Test

The previously mentioned equipment are used to measure the direction of arrival based on a simple outdoor test. The idea is to assure that our DoA setup and code both are reliable when we move the receiving end to outside the campus. In order to achieve that, we implemented a linear antenna array at the receiver which consists of 8 identical telescopic antennas. This antenna is shown in Fig. 4.2.2. The receiving end antenna array is shown in Fig. 4.5.14.

Figure 4.5.14: Linear Antenna Array At The Rx Side

By following the same procedure above, except the transmitted waveform, we managed to capture the data for different positions. For example, we allocated the array in 0 degrees, 30 degrees, 45 degrees, 60 degrees, and 90 degrees. In this allocation we know the angle of departure for the Tx antenna, and we allocated the array accordingly and captured the data for each position. This was to make

sure that, we label the data according to the angle so that, while processing the data using our algorithm, we expect roughly a near angle to what we have positioned the array accordingly. Although, we do not expect the results to be perfect due to the interference and channel effects.

Our transmitted signal is a pulse with 200 μs duration time, 100 μs on time, and 100 μs off time. Our switching time is 600 μs, so for each antenna we capture 3 pulses to make sure at least one of them, usually the middle one, is always full and healthy pulse without any kind of corruption or interference as shown in Fig. 4.5.15. In this figure, we captured around 3 patches of data, as we can notice the silence time in where the switches are off.

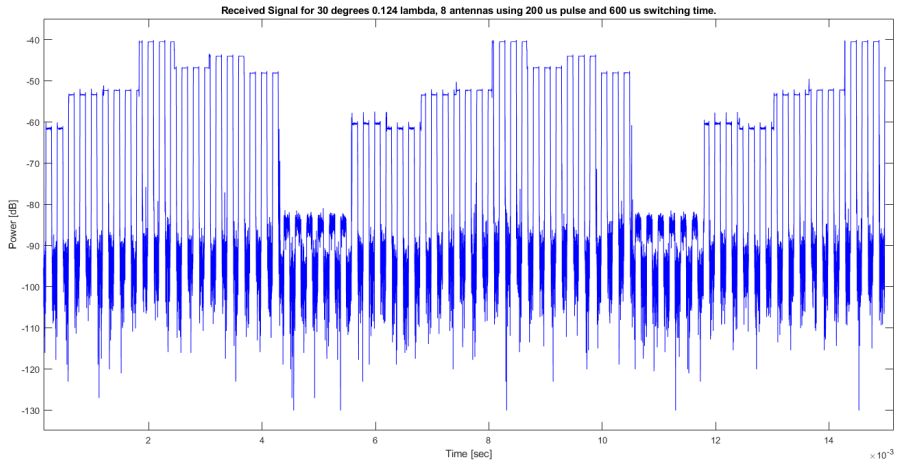

Figure 4.5.15: A received signal in case of DoA using L-Array with spacing element 0.125 lambda

4.5.2.1 Results

For 0.125λ element spacing, using 8 antennas, the results are shown in Fig. 4.5.16, while for 0.25λ element spacing, using 4 antennas, the results are shown in Fig. 4.5.17.

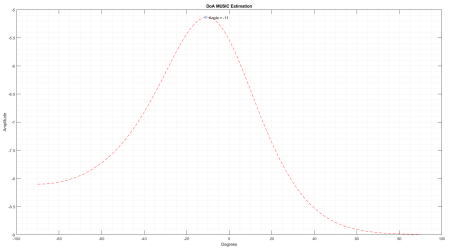

(a) The Angle Corresponding to 30 degrees

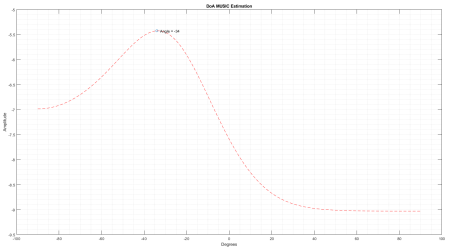

(b) The Angle Corresponding to 45 degrees

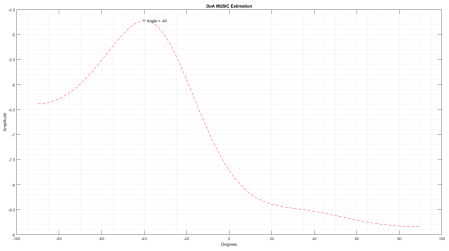

(c) The Angle Corresponding to 60 degrees

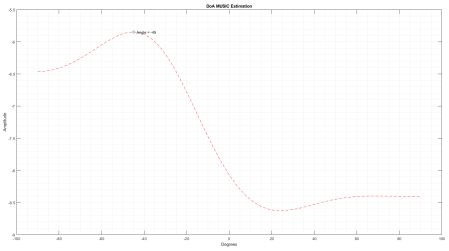

(d) The Angle Corresponding to 90 degrees

Figure 4.5.16: DoA estimation results for 8 elements, with spacing 0.125 lambda.

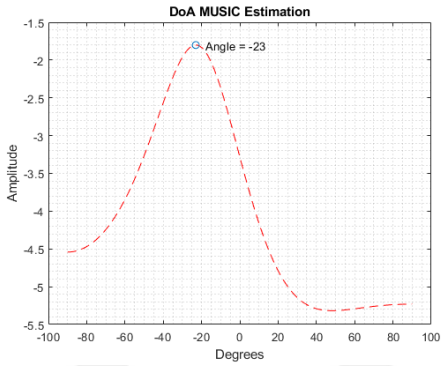

(a) The Angle Corresponding to 30 degrees

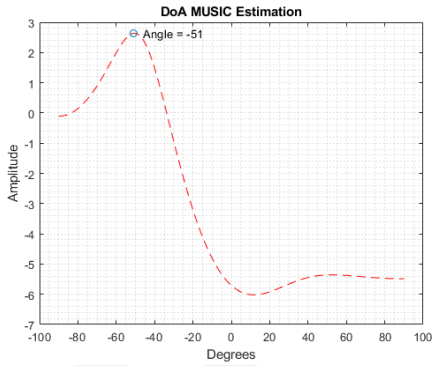

(b) The Angle Corresponding to 45 degrees

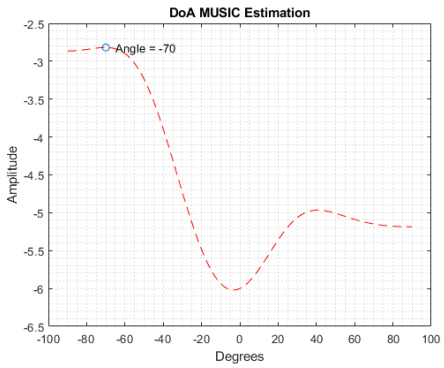

(c) The Angle Corresponding to 60 degrees

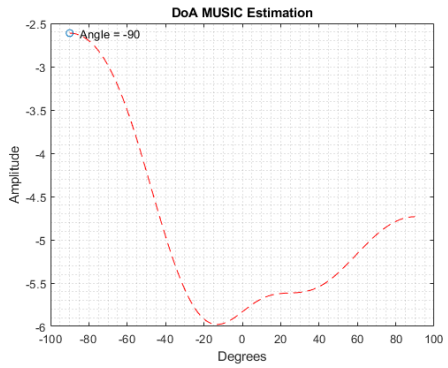

(d) The Angle Corresponding to 90 degrees

Figure 4.5.17: DoA estimation results for 4 elements, with spacing 0.25 lambda.

In general, it is clear that, the angles are being estimated better in case of element spacing = 0.25λ than those in case of element spacing = 0.125λ. This is due to the fact that, when the number of antennas increase the effect of the mutual coupling gets worse as disscused in [46, 47, 38, 45]. However, the accuracy of the angles is not 100% perfect due to the channel effects. Negative degrees are not a concern in our scenario, as the angle comes from the right direction or the left direction, which typically is the same. We also noticed only one peak that corresponds to a single direction of received signals, as expected, due to the fact that, we aligned the array in a line-of-sight location inside the campus just to make sure we do not receive any angles from any NLOS paths.

4.6 Outdoor Setup

In this section we show a highlight of our outdoor setup aided with pictures from the field. Outdoor setup consists of two sides, the Tx side, and the Rx side.

4.6.1 Tx Side

In the Tx side; as described above in Fig. 4.1.2, we have an amplifier connected with the Tx antenna and both are shown in Fig. 4.6.1:

(a) Tx

(b) Tx with Amp

(c) Mini-Circuits Amplifier

Figure 4.6.1: Tx and Amplifier

The cable connecting the transmitter antenna with the power amplifier is $< 1m$ long, as the amplifier is placed near the transmitter antenna on the roof of the Electrical Engineering building at Gebze Technical University. On the other hand, the cable that connects the amplifier with the transmitter device, which is placed in the first floor at the Communications Laboratory, is $> 15m$ long. The losses for this cable is calculated and it introduces a $3.5dB$ loss to the system.

4.6.2 Rx Side

In the Rx side; we have a linear antenna array fixed over the van in case of DoA estimation and a single antenna in case of Doppler spread, CIR, and multipath. A switching circuit with an Arduino controller is connecting the linear array to the R&S FSV Signal and Spectrum Analyzer. In the following Fig. 4.6.2 it is shown the Rx side setup:

(a) Antenna Array Case For DoA

(b) Single Antenna Case

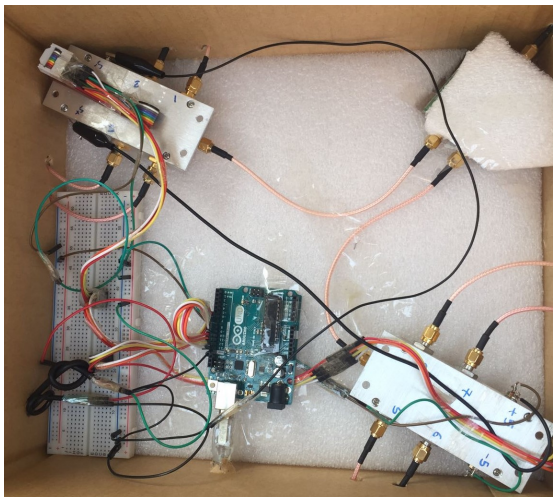

(c) RF Switches With Controller

Figure 4.6.2: Tx and Amplifier

Chapter 5

Data Analysis and Results

To estimate channel parameters, a comprehensive data analysis and processing of the measured data is needed. Our I/Q data as mentioned in 4, does require MATLAB code program to display and calculate the channel impulse responses, multipath power delay profiles, direction of arrivals estimation, K-factor estimation, Doppler spreads estimation, and path loss calculations. In this chapter, algorithms and methods required for each parameter is explained along with the results from the field measured data in separate section.

5.1 Channel Impulse Response

A stochastic, linear, time-varying system is commonly used to model the wireless radio channel. This is also a good model for vehicular channels in which the signal suffers from scattering as a result of the presence of reflecting objects and scatterers in the channel environment. The random change in signal amplitude and phase of the different multipath components, caused by these reflection effects, is one of the factors that causes fluctuations in signal strength, thereby leading to small-scale fading, signal distortion, or both [25].

$$h(\tau, t) = \sum_i a_i(t)\delta(\tau - \tau_i(t)) \tag{5.1}$$

Moreover, small-scale variations of the mobile radio signals are directly related to the channel impulse response of the radio channel. Thus, for a time variant CIR, the passband impulse response is defined as a finite series of attenuated, time-delayed, phase shifted duplicates of the transmitted signal [25, 26]. This passband impulse response of a multipath channel is described by (5.1); where $a_i(t, \tau)$ represent the real amplitudes and $\tau_i(t)$ represent excess delays, for the i^{th} multipath component at time t.

To efficiently characterize a channel, certain metrics for the channel should be utilized from the impulse response. Regularly, we use the impulse response sampled version for the baseband for the caluculations. We propose $h_b[m, n]$ as a discrete equivalent of baseband channels from its passband channel $h(\tau, t)$ [27]. We use the time domain model and get the $a_i(t)$ and $\tau_i(t)$ for each channel realization at a given receiver location. We then average many of these realizations over a period of time to better estimate the delay profile. From the average impulse responses, we then obtain channel power delay profile.

5.2 Multipath Power Delay Profiles

The power delay profiles are obtained by first estimating the channel impulse responses from the I/Q data. This is achieved through cross-correlation with the transmitted m-sequences that are available off-line. This principle of channel estimation by cross-correlation is described in [26] and is depicted in Fig. 5.2.2. The algorithm to obtain channel PDPs is explained in Fig. 5.2.1.

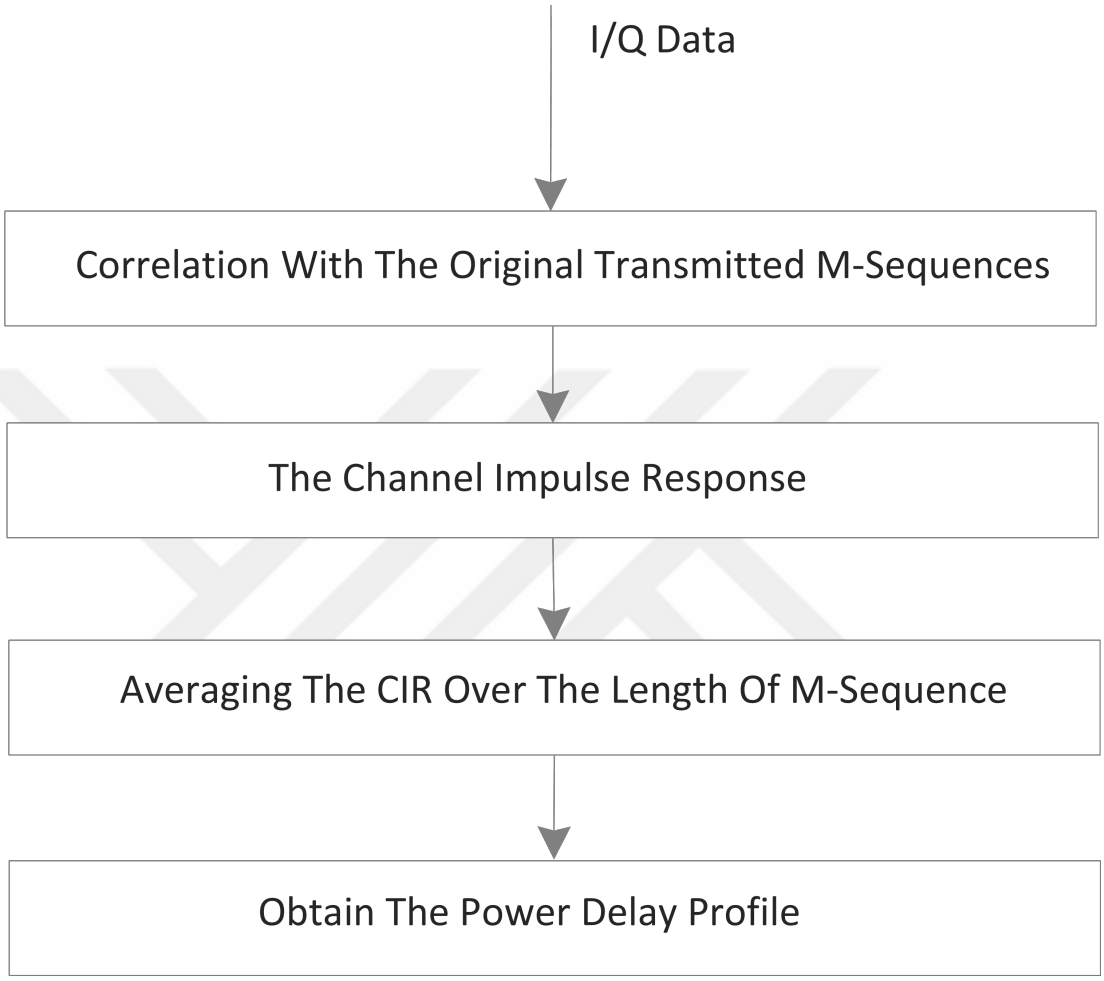

Figure 5.2.1: PDP Algorithm

The algorithm for the CIR averaging is given in Fig. 5.2.1 and it averages the instantaneous CIRs from each m-sequence's cross-correlation. For our measurements, typically there are more than 200 channel measurements in a given received sequence. Mathematically, the averaging process can be described as

$$h_{PDP}[k] = \frac{1}{N_i} \sum_{A=0}^{N_i-1} |h_b[k, LA]| \tag{5.2}$$

where L is the sequence length and N_i is the averaged number of the CIRs. Since the captured data sizes are set to be the same, N_i is fixed in our measurements. The squared samples of the averaged channel impulse response then generates

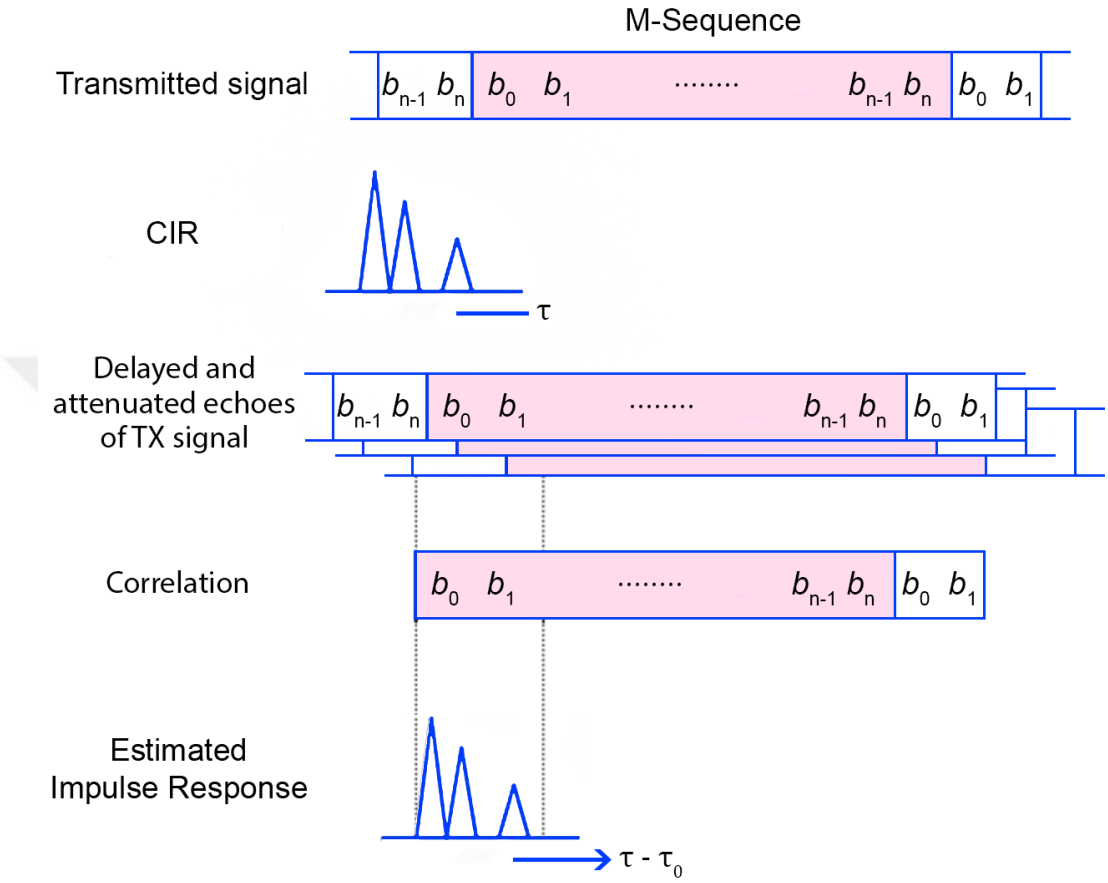

Figure 5.2.2: The principle of channel estimation by cross-correlation.

channel PDP.

5.3 Direction of Arrival

5.3.1 L-Shaped Antenna Array

We use an L-shaped array with 8 elements at various locations as shown in Fig. 5.3.1 A linear uniform array containing $M = 4$ sensors is positioned in the $y-$axis, and similarly another uniform linear array containing $M = 3$ sensors is positioned in the $x-$axis. Taking into consideration that the middle antenna is the

reference antenna, which is a common antenna between both axes. This switched antenna technique is introduced in literature as an alternative to multiple receiver chains . With switched antenna technique, a single receiver can be switched to multiple antennas and therefore can emulate a multiple receiver system. Of course, the received signal needs to be re-adjusted so that the reception at the same time at each antenna is properly emulated [48, 49, 50]. Moreover, the switched antenna system benefits from the sequential sampling process and the flexibility of extending the sensor locations by shifting the antenna system from a location to another without introducing a fixed number of antennas [45].

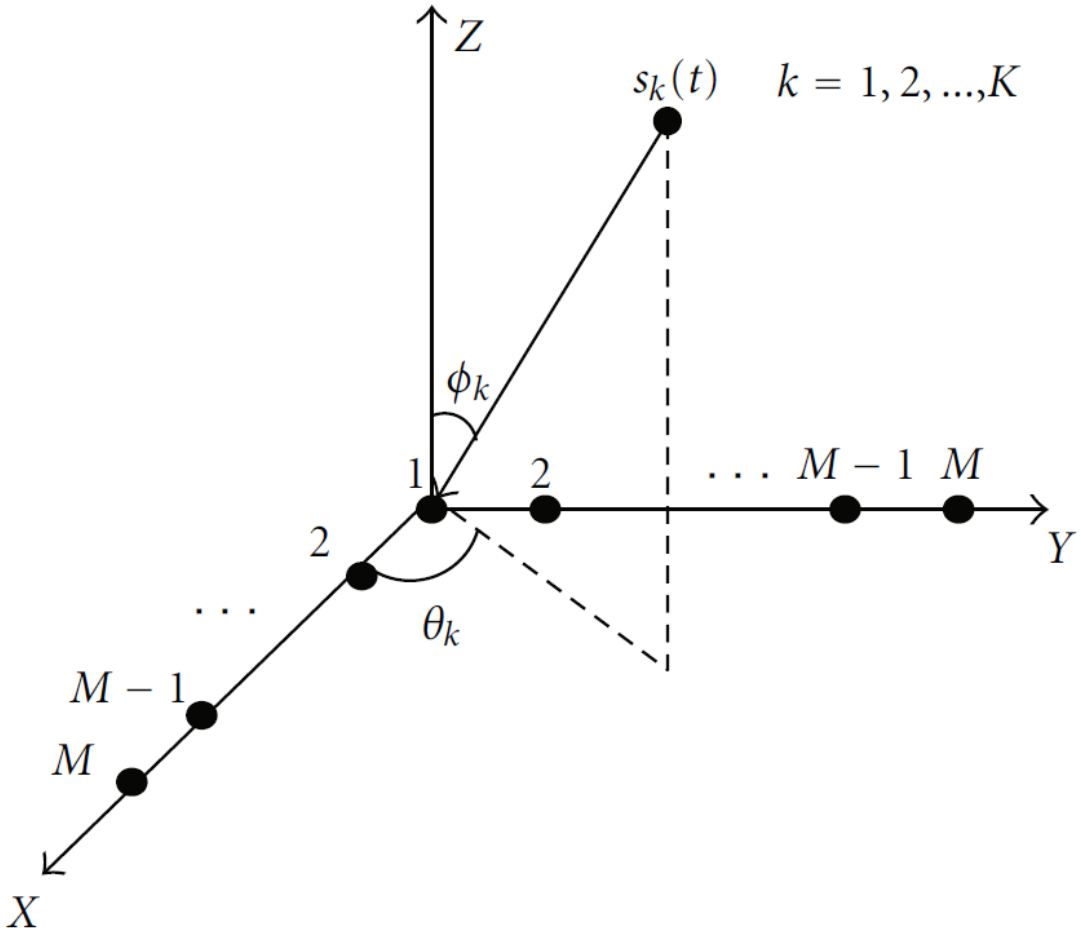

Figure 5.3.1: L-Shape Array

We assume that there are K sources have effect on the $L-$shaped array as

(θ_k,ϕ_k), $k = 1, 2, 3, ..., K$, where ϕ_k and θ_k are the azimuth and the elevation angles of the kth source, respectively. These sources can include LOS (Line Of Sight) path and scattered paths. The received signal of M elements in $x-$axis is

$$x_1(t) = \boldsymbol{A_x s}(t) + \boldsymbol{w_y}(t) \tag{5.3}$$

where $s(t) \in \mathbb{C}^k$ where $s(t) = [s_1(t), s_2(t), ..., s_K(t)]^T$ is the matrix for the source, $w_x(t) \in \mathbb{C}^M$ is an $M \times 1$ vector representing the Gaussian white noise with zero mean and covariance matrix $\sigma^2 M$, and $A_x \in \mathbb{C}^{M \times K}$ is

$$\boldsymbol{A_x} = \begin{bmatrix} 1 & \dots & 1 \\ e^{-j\alpha_1} & \dots & e^{-j\alpha_K} \\ \vdots & \ddots & \vdots \\ e^{-j(M-1)\alpha_1} & \dots e^{-j(M-1)\alpha_K} & \end{bmatrix} \tag{5.4}$$

where $\alpha_k = 2\pi d \cos(\theta k) \sin(\phi k)/\lambda, (k = 1, ..., K)$, d is the spacing for the elements, and λ is the wavelength.

Figure 5.3.2: Rx L-shape Antenna Array

For the y-axis, the received signal formula for M elements is given by

$$\boldsymbol{x_1}(t) = \boldsymbol{A_y}\boldsymbol{s}(t) + \boldsymbol{w_y}(t) \tag{5.5}$$

where $\boldsymbol{w_y(t)}$ is an $M \times 1$ vector representing the Gaussian white noise with zero mean and covariance matrix $\sigma^2 M$, and $\boldsymbol{A_y} \in \mathbb{F}^{M\times K}$ is

$$\boldsymbol{A_y} = \begin{bmatrix} 1 & 1 & \dots & 1 \\ e^{-j\beta_1} & e^{-j\beta_2} & \dots & e^{-j\beta_K} \\ \vdots & \vdots & \ddots & \vdots \\ e^{-j(M-1)\beta_1} & e^{-j(M-1)\beta_2} & \dots e^{-j(M-1)\beta_K} & \end{bmatrix} \tag{5.6}$$

where $\beta_k = 2\pi d \sin(\theta_k)\sin(\phi_k)/\lambda, k = 1, ..., K$. $\boldsymbol{x_1}(t) \in \mathbb{C}^M, \boldsymbol{x2(t)} \in \mathbb{C}^M, \boldsymbol{A_x} \in \mathbb{C}^{M\times K}$ and $\boldsymbol{A_y} \in \mathbb{C}^{M\times K}$.

On the other hand, for the $L-$shaped array; the received signal is given by

$$\boldsymbol{x(t)} = \begin{bmatrix} \boldsymbol{x_1(t)} \\ \boldsymbol{x_2(t)} \end{bmatrix} = \begin{bmatrix} \boldsymbol{A_x} \\ \boldsymbol{A_y} \end{bmatrix} \boldsymbol{s}(t) + \boldsymbol{w}(t) = \boldsymbol{A}\boldsymbol{s}(t) + \boldsymbol{w}(t) \tag{5.7}$$

where $\boldsymbol{A}$ and $\boldsymbol{w(t)}$, the direction matrix and the noise matrix are represented by the following matrices:

$$\boldsymbol{A} = \begin{bmatrix} \boldsymbol{A_x} \\ \boldsymbol{A_y} \end{bmatrix}, \boldsymbol{w(t)} = \begin{bmatrix} \boldsymbol{w_1(t)} \\ \boldsymbol{w_2(t)} \end{bmatrix} \tag{5.8}$$

For the data model obtained in (5.7), we will use MUSIC algorithm to estimate the DoA [51]. MUSIC algorithm is asymptotically efficient and propose an excellent performance for narrow band signals [52]. MUSIC algorithm can also be applied to whether arbitrary arrays, as well as uniform linear arrays or circular arrays [53, 54].

The correlation matrix for ((5.7)) is of the form

$$\begin{aligned} \boldsymbol{R} &= E[\boldsymbol{x_k}\boldsymbol{x_k}^{\boldsymbol{H}}] \\ &= E[(\boldsymbol{A}\boldsymbol{s}(t) + \boldsymbol{w}(t))(\boldsymbol{A}\boldsymbol{s}(t) + \boldsymbol{w}(t))^{\boldsymbol{H}}] \\ &= \boldsymbol{A}E[\boldsymbol{s}(t)\boldsymbol{s}(t)^{\boldsymbol{H}}]\boldsymbol{A}^{\boldsymbol{H}} + E[\boldsymbol{w}(t)\boldsymbol{w}(t)^{\boldsymbol{H}}] \\ &= \boldsymbol{A}\boldsymbol{P}\boldsymbol{A}^H + \sigma^2\boldsymbol{I} \end{aligned} \tag{5.9}$$

where $\mathbf{P}$ is the signal correlation matrix, σ^2 is the white noise power (variance) and $E[.]$ is the expectation operator. The covariance matrix is then calculated from,

$$\boldsymbol{R} = \frac{1}{n} x x^H, \tag{5.10}$$

where n is the length of x. Although, the eigen decomposition techniques make use of (5.7) to get the directions of arrival. Though, this is only valid when $\mathbf{R}$ is a full rank matrix. However, when the signals are coherent as in our scenarios as we have multipaths, the previously mentioned relations are no longer valid. In this case, we use spatial smoothing forward and backward to take multipath scatterings into consideration. We performed the forward and backward spatial smoothing after getting the covariance matrix in (5.10) as in [55], using MATLAB. In Fig. 5.3.3, the DoA estimation system model done by MATLAB is described.

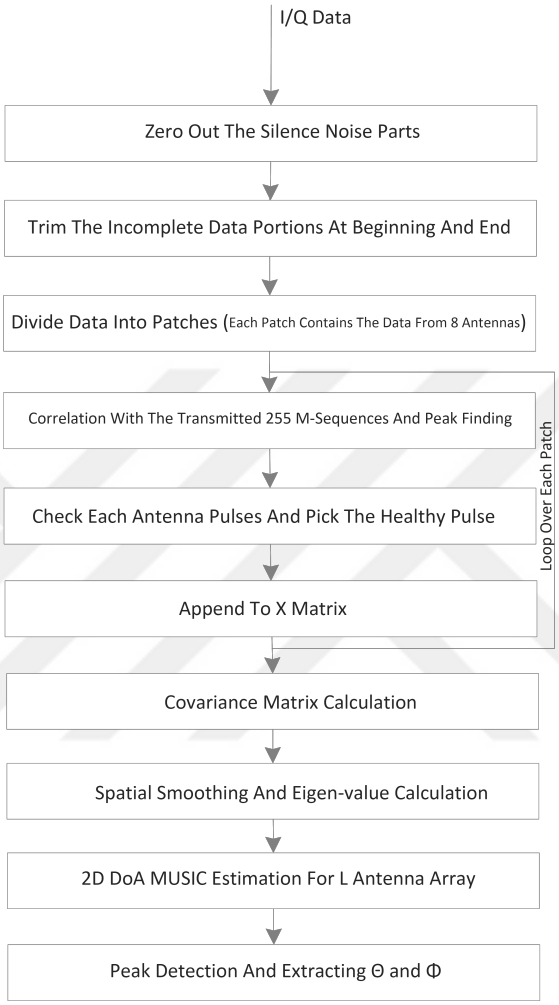

Figure 5.3.3: DoA Estimation System Model

The noise subspace used in MUSIC is then obtained from the eigenvalue decomposition of the smoothed covariance matrix. We now have the means to solve for the incident signal mode vectors. If E_N is defined to be the $M \times N$ matrix whose columns are the N noise eigenvectors. We calculated the MUSIC Pseudo-spectrum as the following expression,

$$\boldsymbol{P_{MU}}(\theta, \phi) = \frac{1}{\boldsymbol{a^*}(\theta, \phi)\boldsymbol{E_N}\boldsymbol{E_N^*}\boldsymbol{a}(\theta, \phi)} \tag{5.11}$$

After estimating the Pseudo-spectrum, a peak detection is used to calculate

the azimuth $\mathbf{\Phi}$ and the elevation $\mathbf{\Theta}$ angles as the following eq. (5.12)

$$\mathbf{\Theta} = \begin{bmatrix} \theta_0 \\ \theta_1 \\ \vdots \\ \theta_k \end{bmatrix}, \mathbf{\Phi} = \begin{bmatrix} \phi_0 \\ \phi_1 \\ \vdots \\ \phi_k \end{bmatrix} \tag{5.12}$$

where each θ_k and ϕ_k is a different angle from different direction due to scattering behavior of the channel.

5.3.2 Linear Antenna Array

We consider only 5antenna elements in this case, we take the linear elements of the $L-$shape array and use the same algorithm described above but for only one direction and one angle. As we cannot resolve azimuth and theta altogether from a linear array, the same matrices and equations are valid but with dimension reduced to 1 instead of 2.

Hence, the MUSIC Pseudo-spectrum is reduced to be as the following expression 5.13,

$$\boldsymbol{P_{MU}}(\theta, \phi) = \frac{1}{\boldsymbol{a}^*(\theta)\boldsymbol{E_N}\boldsymbol{E_N^*}\boldsymbol{a}(\theta)} \tag{5.13}$$

In conclusion, both L-shape antenna array and linear antenna array were used to estimate DoA using MUSIC algorithm. We presented the mathematical expressions for both of the cases in details. MUSIC algorithm described in 5.3.3 is implemented by the authors using MATLAB for the both cases. The processing for the I/Q data is done offline for each receiver location for each point on the map in Fig. 4.4.1. Noticing that, some I/Q data at certain receiving locations, especially those in NLOS locations, are corrupted due to the large noise level. Thus, for those points, we could not resolve our signal to feed it to the algorithm. Therefore, those data for those locations were neglected. Another key of the channel characteristic is the K-Factor. In the next section, K-Factor estimation is discussed in details.

5.4 Rician K-Factor

Since Ricean K-Factor is an indication for the relative strength of the scattered components and the direct components of the received signal, it provides important information for the quality of the channel link. Hence, Ricean K-Factor is one of the essential and required key parameters for the channel modeling [56]. Thus, it is of a great importance that the K-Factor for the FM radio channels needs to be deeply analyzed.

The effect of shadowing and path loss must be eliminated as a first step. This is due to the fact that the K-factor is actually a parameter that outlines the small-scale fading of the wireless channel. It is already done in section 5.2 , where CIRs collected and PDP is obtained. Since our bandwidth is 1 MHz, which is considered as wideband, as discussed in [57]; we can obtain the K-Factor for different delay bins and different bandwidths in regard to the reconstructed CIRs as in Eq. (5.14):

$$\hat{K_w}(\tau, t) = \frac{\sqrt{E^2(P) - Var(P)}}{E(P) - \sqrt{E^2(P) - Var(P)}} \tag{5.14}$$

where $E(.)$ and $Var(.)$ represent the expectation and variance of (.), respectively and τ represents the i-th delay bin. P denotes the CIRs power, which can be denoted as

$$P = |h(\tau, t)|^2 \tag{5.15}$$

5.5 Doppler Spread

In our measurement site, for Doppler measurements, the transmission is between a fixed base station antenna, located on top of a the electrical engineering building at Gebze Technical University, and a mobile receiver on top of the SUV down on the highway. The channel link between the Tx and the Rx is typically containing

buildings, which affect the transmitted signal by scattering or reflection. The channel link is almost stationary only when the SUV is stopped. Moreover, the transmission to a moving vehicle is usually introducing a time-varying channel link. Thus, due to scatter paths at arriving to the SUV from different arriving angles, different Doppler shifts occur. For each angle of arrival associated with each received path, the Doppler shift will change by different amounts [29].

It is well known that, if the signal is arriving ahead of the SUV the Doppler shift will be positive, while the arriving signals from behind will be negatively shifted by the same amount [29]. Generally, Doppler shift information is useful for the communication system analysis and for understanding the multipath structure of the channel as discussed in [29].

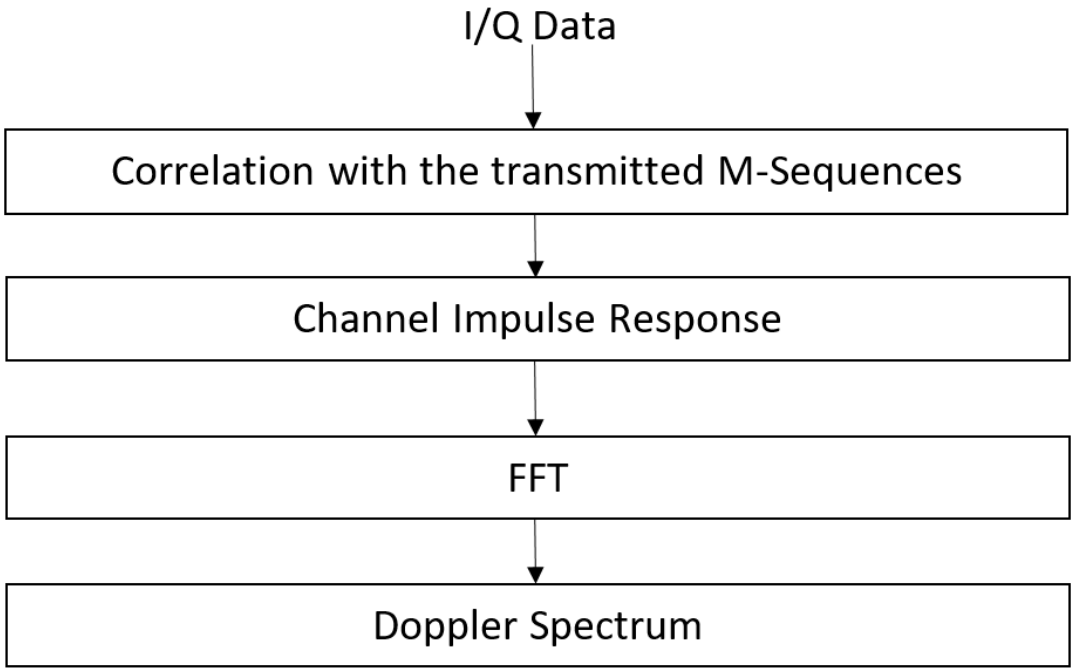

Figure 5.5.1: Doppler Spectrum Algorithm

On the other hand, in order to obtain the Doppler spectrum, two simple steps are performed on the data as in Fig. 5.5.1. Firstly, channel correlation function is computed hence the autocorrelation between the transmitted sequence and the received I/Q complex data array is calculated. Secondly, applying fast Fourier

transform (FFT) to the channel correlation function obtained in the previous step results in the Doppler spectrum [58, 59].

5.6 Path Loss

For any wireless communication system, the propagation path loss is defined as the losses that exist in the channel between the transmitter and the receiver. That puts the pass loss in a very important place among the channel characteristics as it is an essence for the design and analysis of the wireless communication systems. Typically, the transmitter waves does not directly reach to the receiver. This is due to the channel effect which includes obstacles, buildings, and vegetation which block the direct LOS path. The received propagation signals are mainly suffering from a lot of reflection, diffraction, scattering and Doppler effect as discussed in [25].

Moreover, the definition of the path loss can be defined as a ration. This ratio is between transmitted and received power as shown in[60] (5.16):

$$PL(d) = PL(d_0) + 10nlog_{10}(d/d_0) \tag{5.16}$$

where, d is the distance between the receiver and the transmitter, d_0 is the reference distance (usually taken at Rx1), and n is the path loss exponent.

The path loss exponent for the free space path loss is typically equal to 2. The path loss exponent is an indication for the rate of increasing the path loss w.r.t the distance. On the other hand, to obtain PL, distance between Tx And Rx points has been obtained using collected longitudes and latitudes for each Rx point, while PL exponent is calculated individually for each receiving location using least square criteria between estimated values and measured values for different captured data for the same receiver location. From the site in Fig. 4.4.1 Rx1 is taken to be the reference distance. All done through feeding the I/Q data into

MATLAB code simulation.

5.7 Results

5.7.1 Transmitted Signal

The transmitted signal center frequency is 86 MHz, with a bandwidth of 1 MHz. Two different signals has been transmitted according to different receiver antennas.

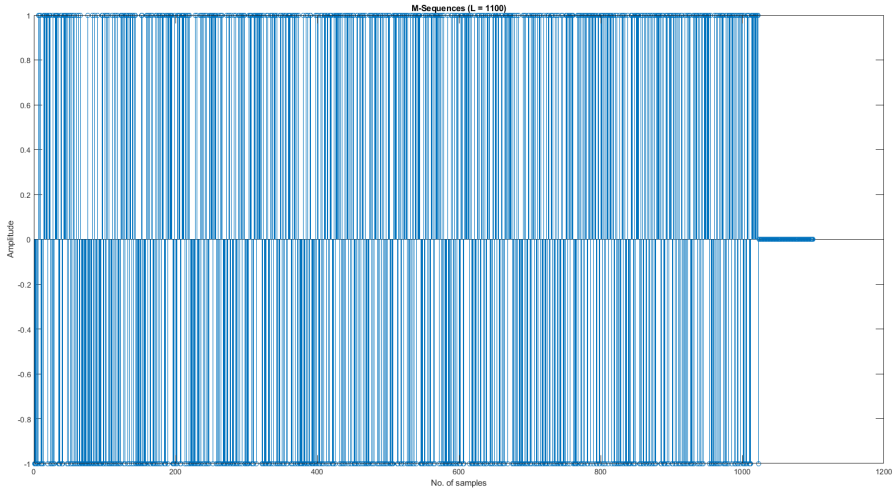

Figure 5.7.1: Transmitted M-Sequence

5.7.1.1 For Single Antenna Receiver

For the case of multipath measurements, our baseband transmitted signal is a typical maximum-length (m-sequences) [26] of length $L = 2^m - 1$. We use the sequence length $L = 1023$ ($m = 10$) and the sequence chips has a transmission rate of $1x10^6$ Sample Rate/Hz, the chip duration is $T_c = 1$ μs. The sequence was padded with zeros until $L = 1100$, hence the sequence is being continuously

repeated for $T_s = 1100\mu s$. We generated the sequence using MATLAB and converted it to ".wv" file format and then uploaded it to the transmitter, thanks to the R&S ARB Toolbox PLUS V 2.4 software. The transmitted signal is shown in Fig. 5.7.1.

5.7.1.2 For L-shape and Linear Shape Switched Antenna Arrays Receivers

For the case of DoA measurements, our transmitted signal is also a maximum-length (m-sequences) as in case of multipath, but with $M = 8$ antennas. The m-sequences were transmitted at same rate of $1x10^6$ sample rate/Hz, the chip duration is $T_c = 1$ μs. The sequence then was padded with zeros for $L = 300$ samples. Hence, the sequence is being continuously repeated every $Ts = 300$ μs.

5.7.2 Received Signal

5.7.2.1 For Single Antenna Receiver

In order to capture the received signal by the receiver, we utilized the R&S IQ Wizard of R&S spectrum analyzer. The captured I/Q data is then imported to MATLAB for further processing and analysis.

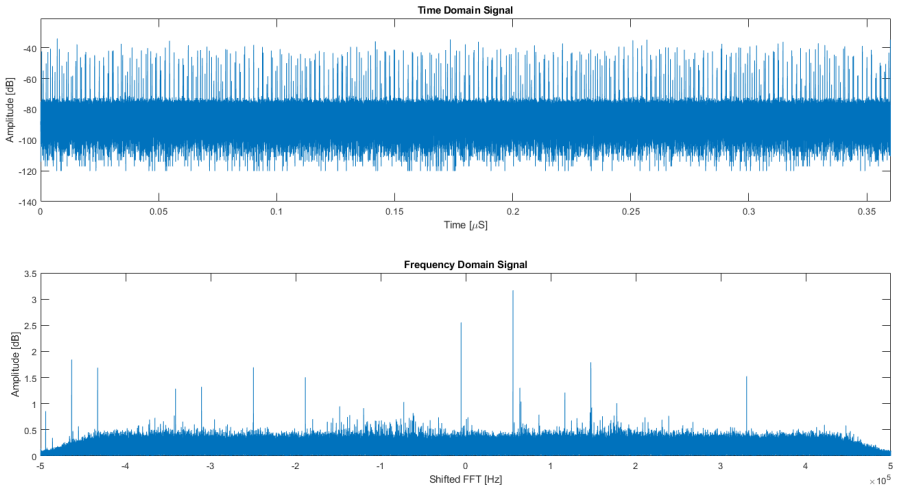

Figure 5.7.2: Received Signal

5.7.2.2 For L-shape and Linear Shape Switched Antenna Arrays Receivers

For DoA measurements, the readings from each antenna are needed independently. Typically, we need as many RF chains as the number of the antennas for DoA measurements. However, in this study, we used only a single RF chain but then switched between the antenna elements. The switching is accomplished via RF switches, where we used two 4x1 switches (Mini-Circuits switch ZSWA-4-30DR) with a direct contact to 8 receive antennas. We also needed a $2x1$ splitter/combiner (Analog Devices switch HMC574AMS8E) to switch the input from each 4x1 switches to the R& S FSV Signal and Spectrum Analyzer. The controlling of the switches were performed via a microcontroller. RF switches and their controlling circuit is shown in Fig. 4.6.2. A sample received signal is shown in Fig. 5.7.3

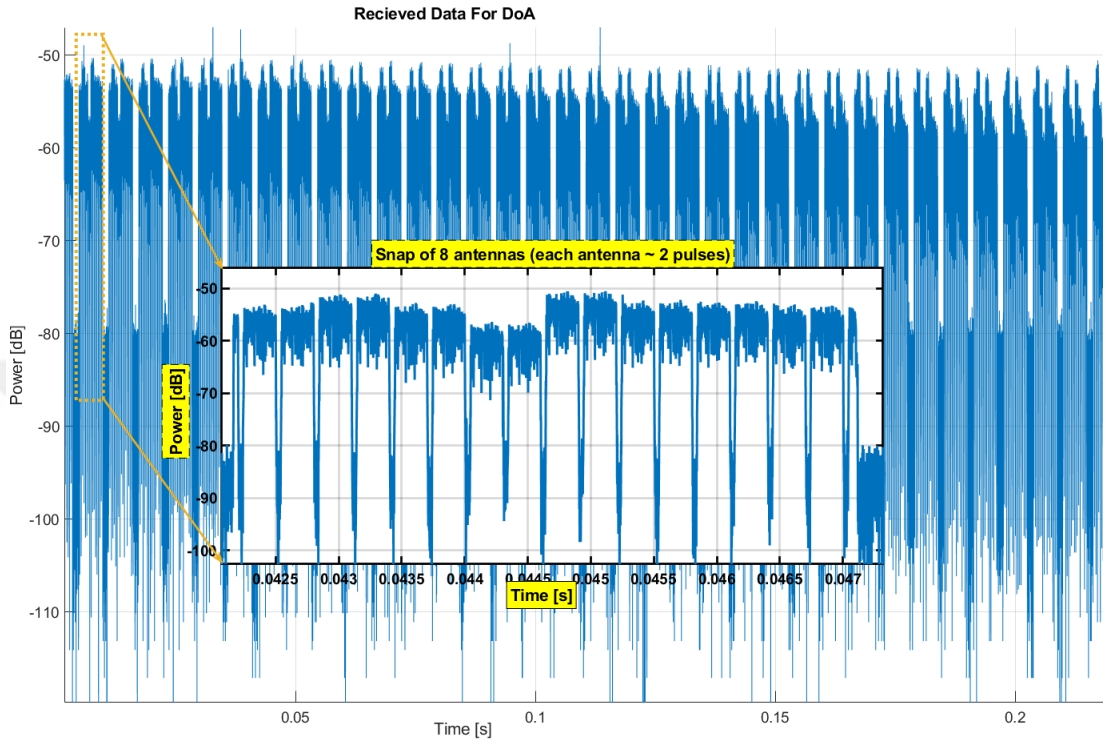

Figure 5.7.3: Received Signal

In order to keep track of synchronization in case of losing the GPS synchronization, the micro-controller is programmed so as to provide a silence time in which the switching circuit is blocking the signal. This is clearly shown in Fig. 5.7.3, which is represented by the silent white spaces between each patch. Furthermore, to align all the pulses as if they are received at the same time, we shift the phase component for each pulse to introduce shift in time. Hence, we establish the synchronization.

5.7.3 Multipath Delay Profiles

Since the measurement sites included different types of environments, we have encountered different channel impulse responses. For the measurement campaign carried out in the site given in Fig. 4.4.2, we mostly obtained channel PDPs that either had a strong single multipath or another surviving multipath component

nearby the first one. These two cases are shown in Figs. 5.7.8 and 5.7.9. Hence, as we move away from the transmitter in the urban environments, the clusters through which we receive the signals decreases. This agrees with the stochastic channel models developed for COST-259 [61] and for the FM Band channel models [62].

As for the site given in Fig. 4.4.1, we have obtained different channel PDPs for different environments. For the case of a rural environment, we have obtained a strong line-of-sight component as given in Fig. 5.7.4.

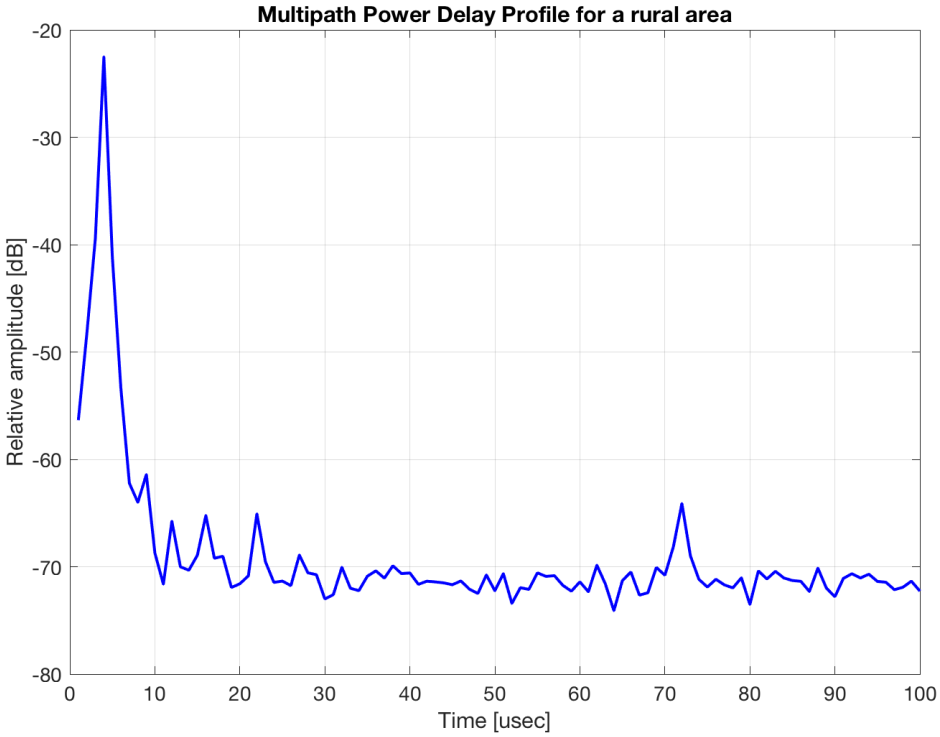

Figure 5.7.4: PDP for site in Fig.4.4.1 receiver location 25.

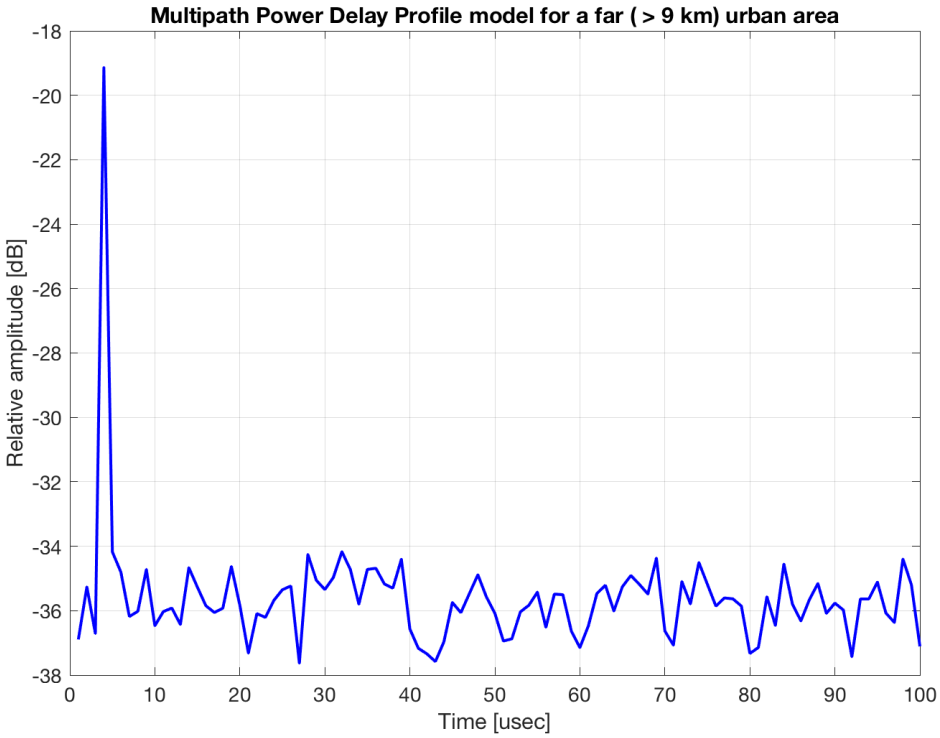

Figure 5.7.5: PDP for site in Fig.4.4.2 receiver location 28.

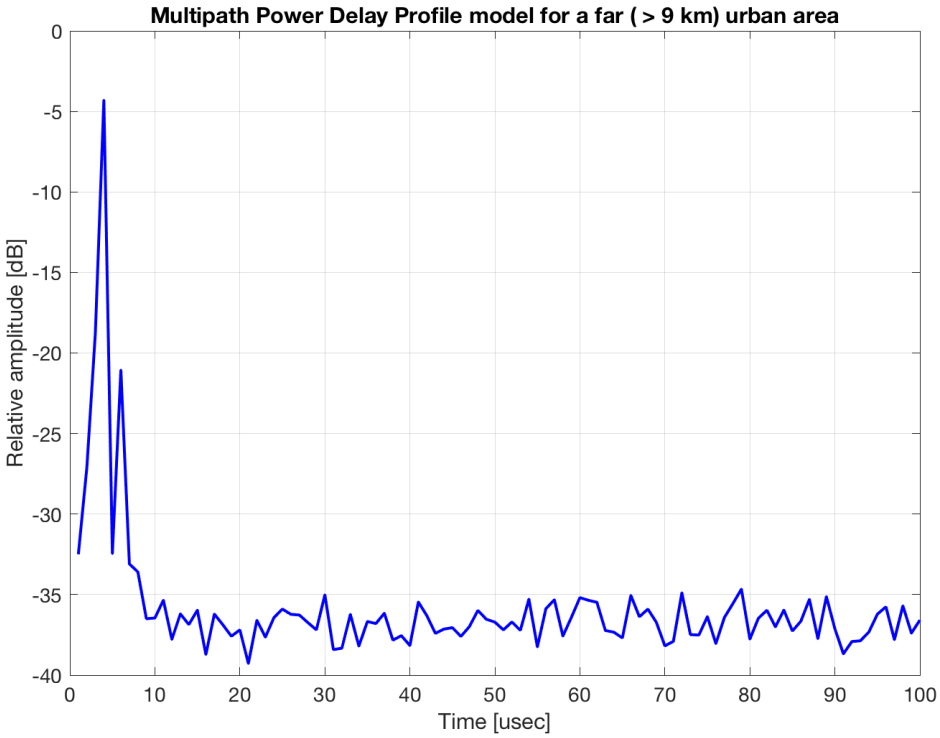

Figure 5.7.6: PDP for site in Fig.4.4.2 receiver location 5.

When the measurement points are chosen from the urban areas, we started receiving more clusters and consequently we observed larger channel excess delays. These are shown in Figs. 5.7.5 and 5.7.6. For the case of Fig. 5.7.9, we have observed channel excess delays as large as 30 μs, though the last pack of multipaths were 25 dB lower than the strongest path. Moreover, for the case of Fig. 5.7.7, we observe the same as in Figs. 5.7.5 and 5.7.6.

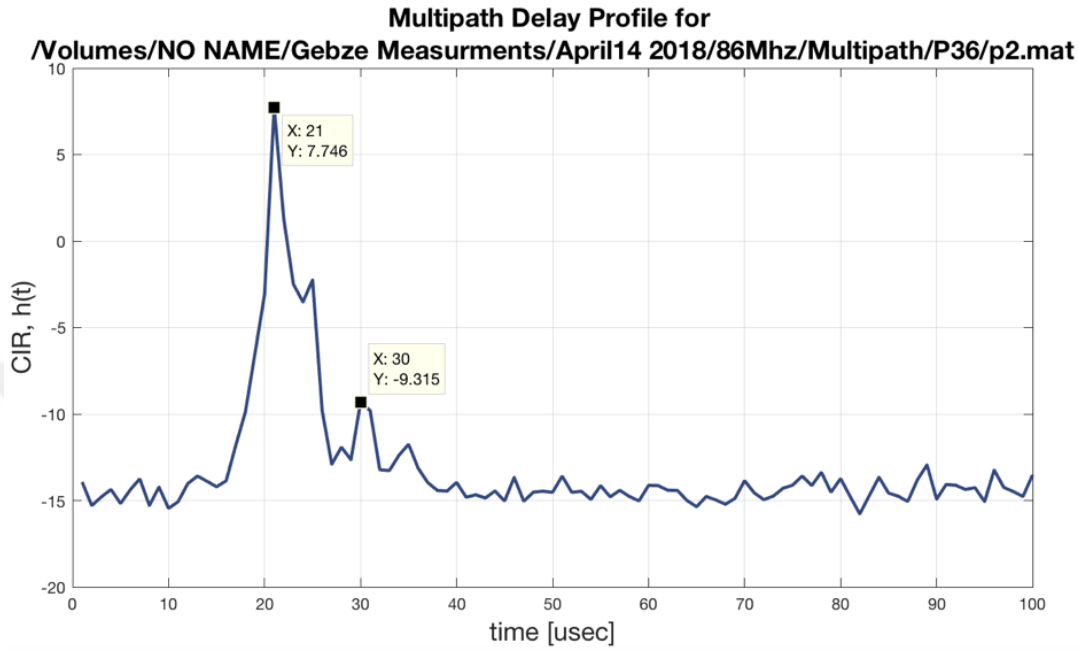

Figure 5.7.7: PDP for site in Fig.4.4.1 receiver location 36.

Although the PDPs obtained through this study are in good agreement with COST-207 channel models [63], for bad urban case, we have obtained channels with more clusters and larger excess delays. Hence, for the FM band with bad urban environment, we recommend the channel PDP model given in Fig. 5.7.10.

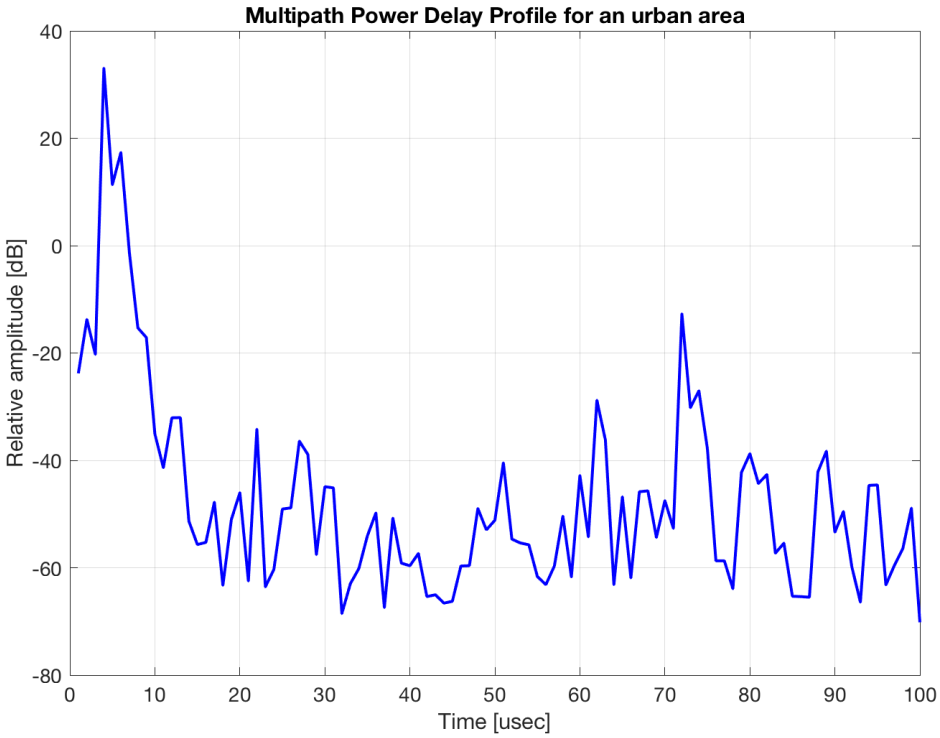

Figure 5.7.8: PDP for site in Fig.4.4.2 receiver location 74.

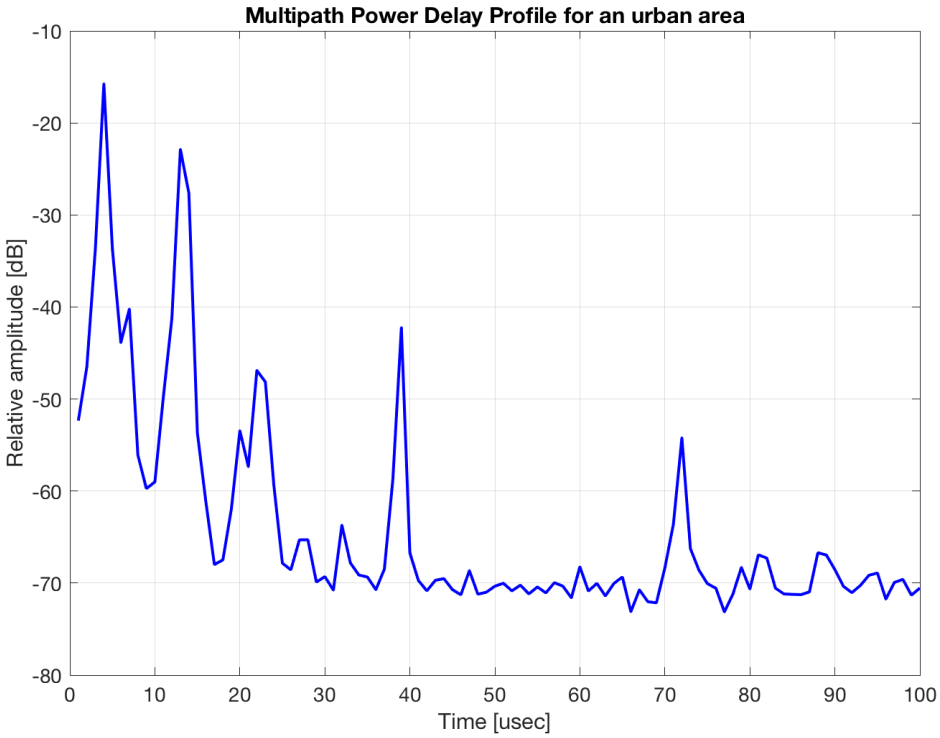

Figure 5.7.9: PDP for site in Fig.4.4.2 receiver location 71.

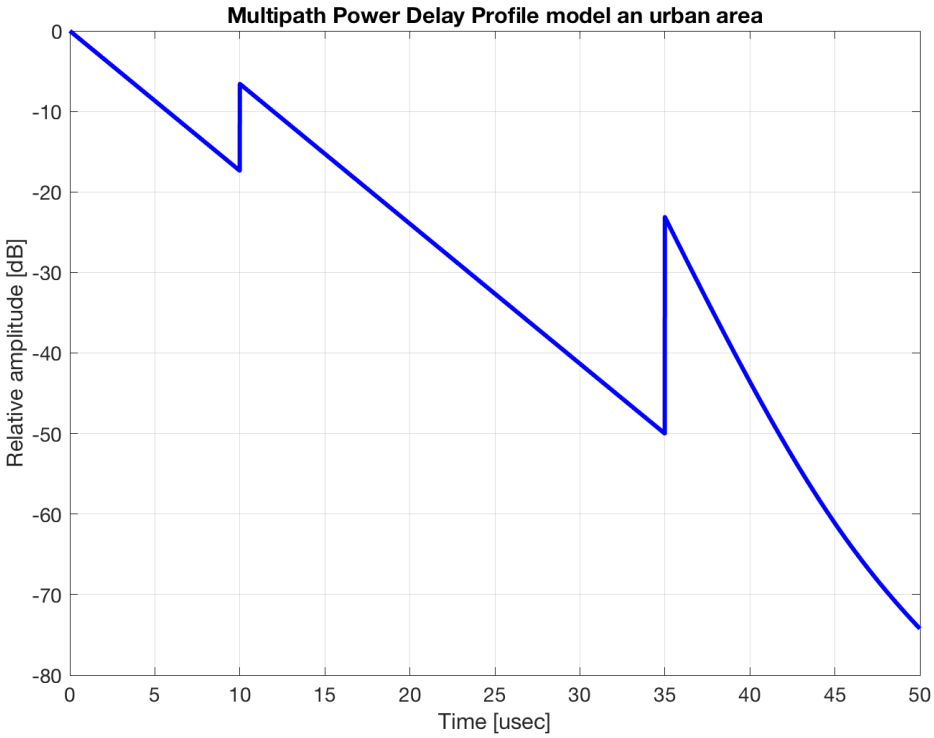

Figure 5.7.10: FM band channel PDP model for bad urban environment.

For the hilly terrain regions, we have picked two receiver locations that present the typical behavior. Figures. 5.7.11 and 5.7.12 show the channel PDP for these two cases. As can be observed, for the hilly terrain regions, we typically get multipath components and channel excess delays beyond 10 μs. Although most of the hilly terrain environment measurements are in agreement with COST-207 hilly terrain channel models [63], for some cases we have observed additional channel clusters. In order to model this behavior, we propose the channel PDP model given in Fig. 5.7.13.

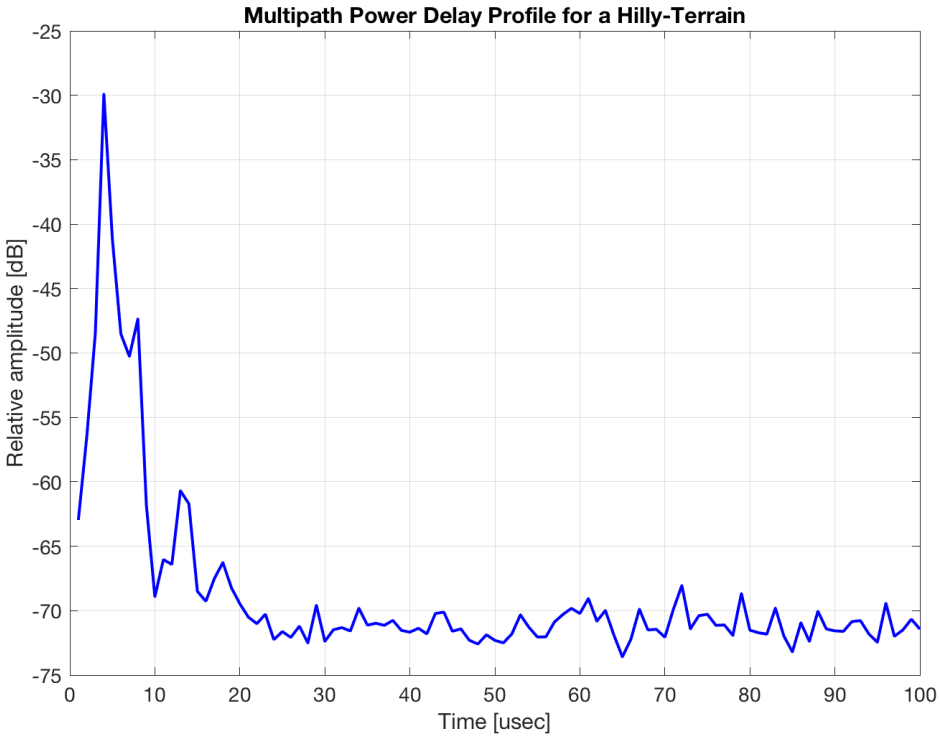

Figure 5.7.11: PDP for site in Fig.4.4.1 receiver location 36.

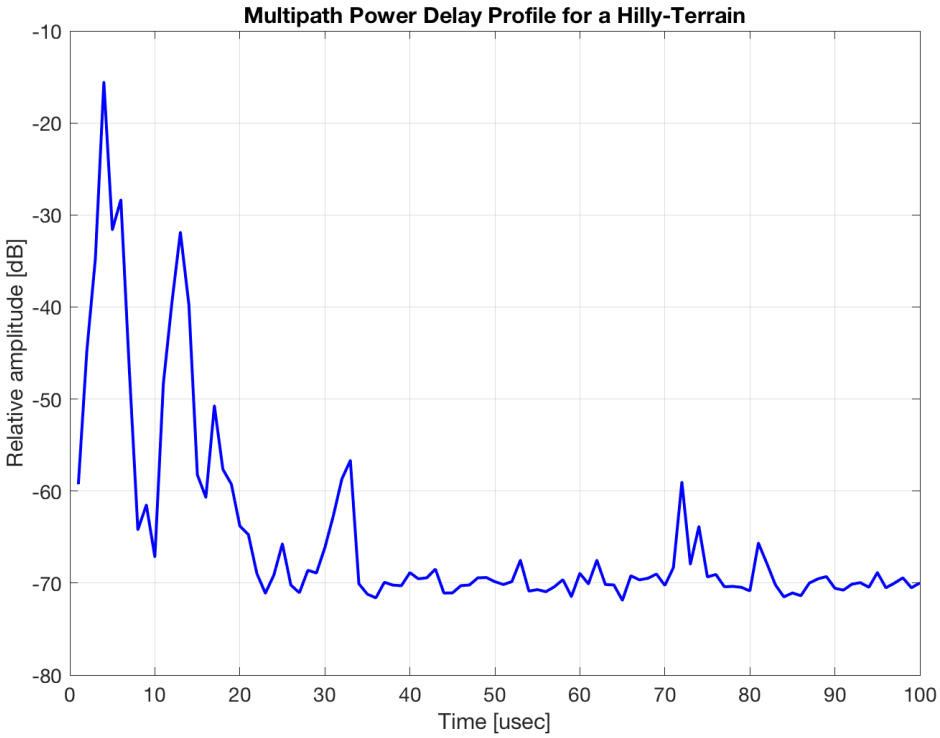

Figure 5.7.12: PDP for site in Fig.4.4.1 receiver location 37.

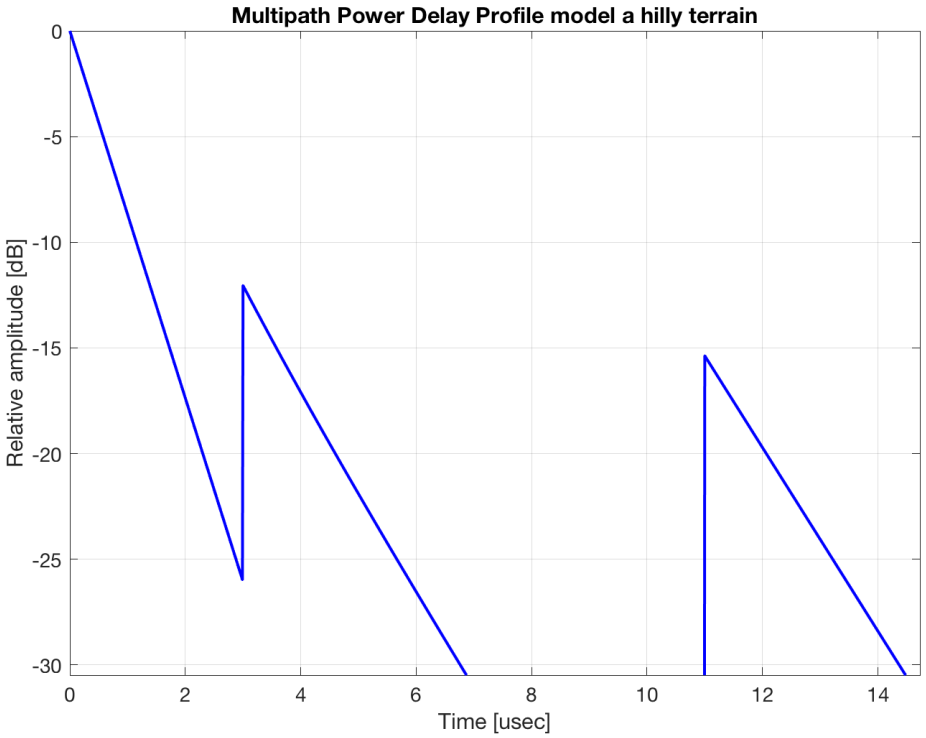

Figure 5.7.13: FM band channel PDP model for a multi-cluster hilly terrain environment.

5.7.4 Direction of Arrival

5.7.4.1 L-Shape Antenna Array

For the same receiver location given for the PDP graph 5.7.7, we also analyzed the incoming angles. The DoA estimation is given in Fig. 5.7.14. As can be seen we have signals mainly coming from one direction, but the angle spread is large due to strong reflections around the receiver.

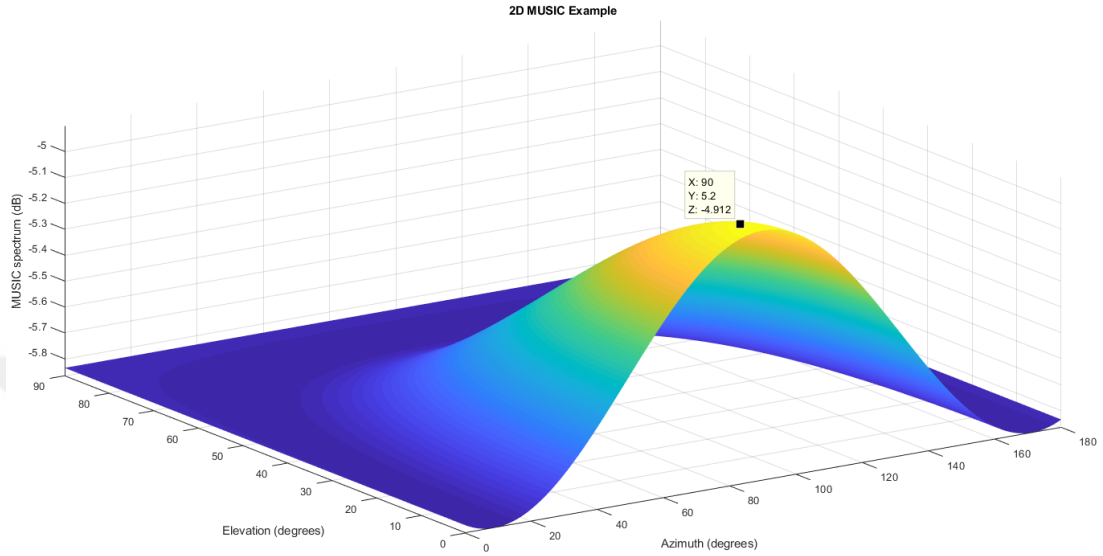

Figure 5.7.14: DoA for a strong LOS receiver location.

5.7.4.2 Linear Antenna Array

For the vicinity of 5 Km site in Fig.4.4.1, many locations are used for linear antenna array. The DoA estimation for some points are given in the following Figs.5.7.15,5.7.16,5.7.17,5.7.18,5.7.19,5.7.20.

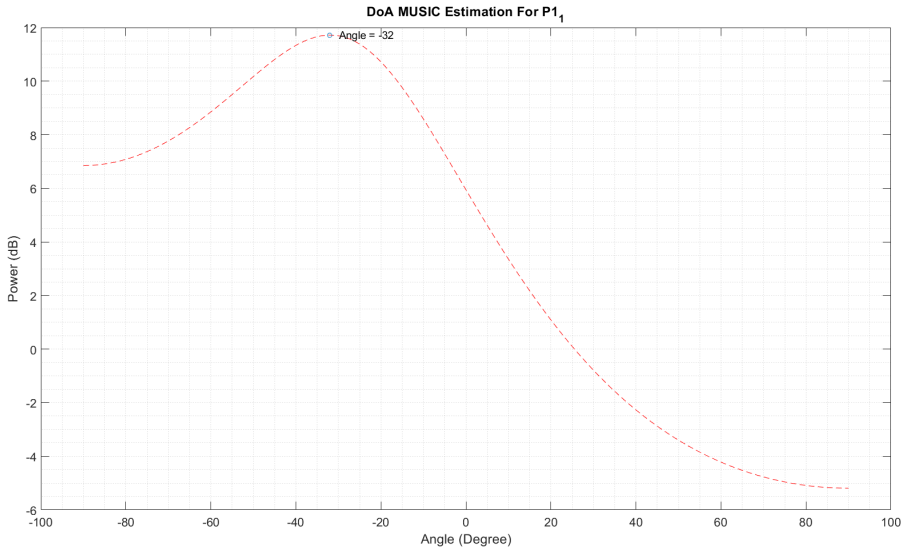

Figure 5.7.15: DoA for site in Fig.4.4.1 receiver location 1.

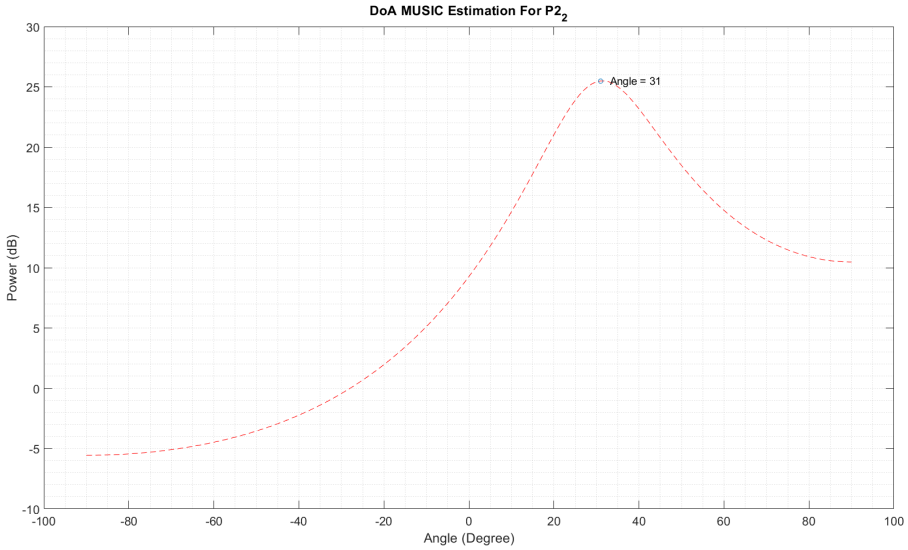

Figure 5.7.16: DoA for site in Fig.4.4.1 receiver location 2.

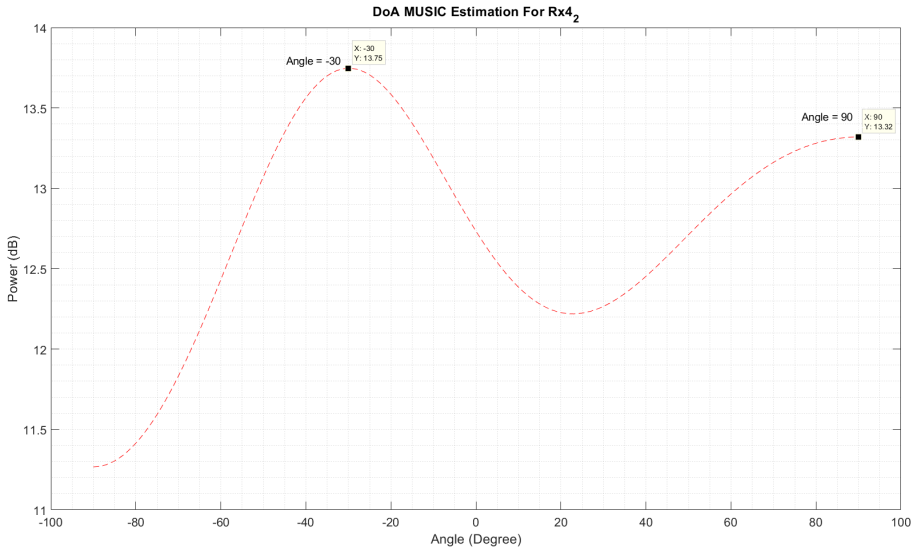

Figure 5.7.17: DoA for site in Fig.4.4.1 receiver location 4.

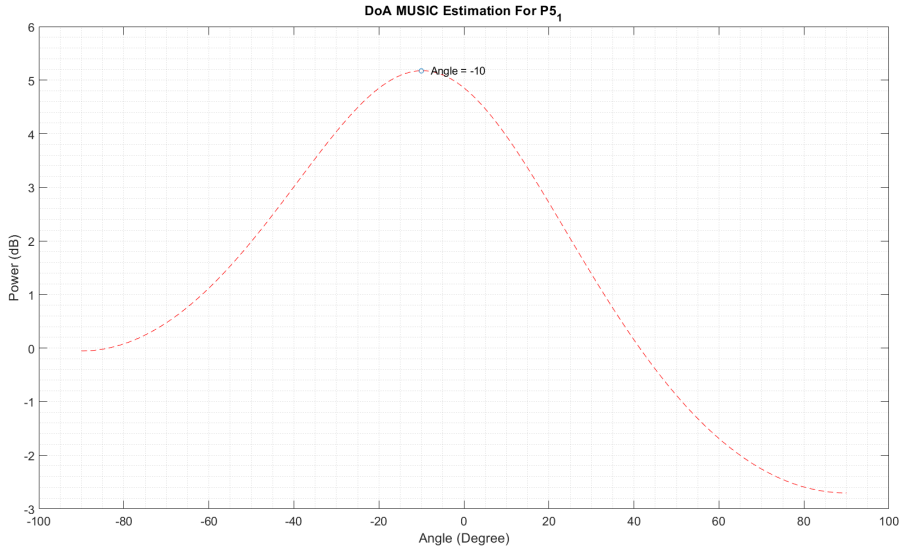

Figure 5.7.18: DoA for site in Fig.4.4.1 receiver location 5.

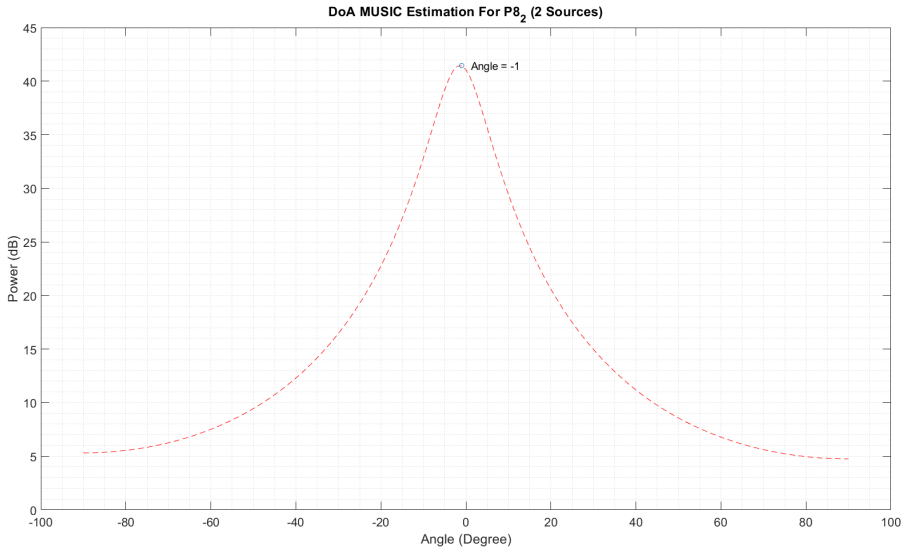

Figure 5.7.19: DoA for site in Fig.4.4.1 receiver location 8.

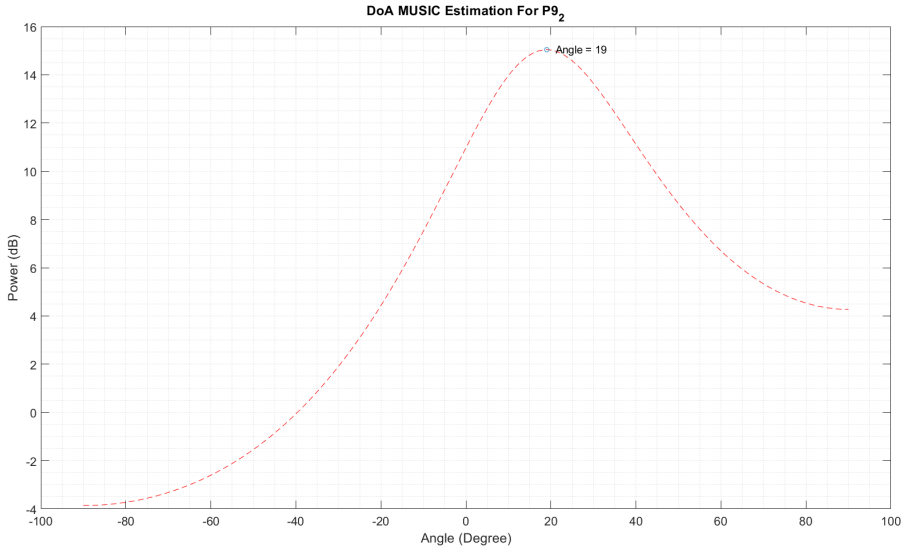

Figure 5.7.20: DoA for site in Fig.4.4.1 receiver location 9.

As we notice from the previous figures, in most of the scenarios we encounter a strong LOS path, as a result, a single DoA is estimated. Moreover, in Fig. 5.7.17 , we encountered a second strong multipath represented in the second angle shown

in the figure. Furthermore, For the the L-shape array, the angle spread is large due to strong reflections around the receiver.

5.7.5 Ricean K-Factor

5.7.5.1 Distances less than 5 km

For the vicinity of 5 km (75 Rx points), the K-Factor is shown versus the statistics of the received amplitude and versus the Rx locations in the following Fig. 5.7.21

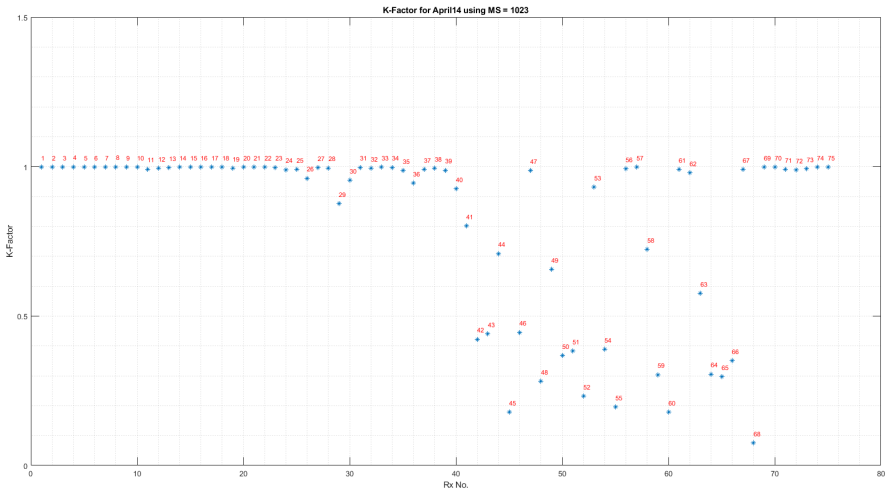

Figure 5.7.21: K-Factor of each Rx point.

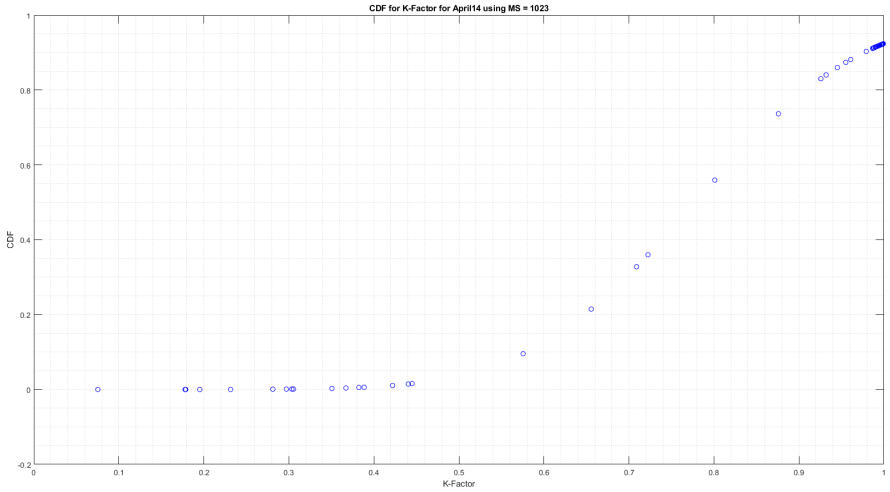

Figure 5.7.22: The statistics of the received amplitude and K-Factor

5.7.5.2 Distances around 9.5 km

For the vicinity of 9.5 Km (33 Rx points), the K-Factor for each receiver location is shown in Fig. 5.7.23, while the statistics of the received amplitude for each receiver location is shown in Fig. 5.7.24.

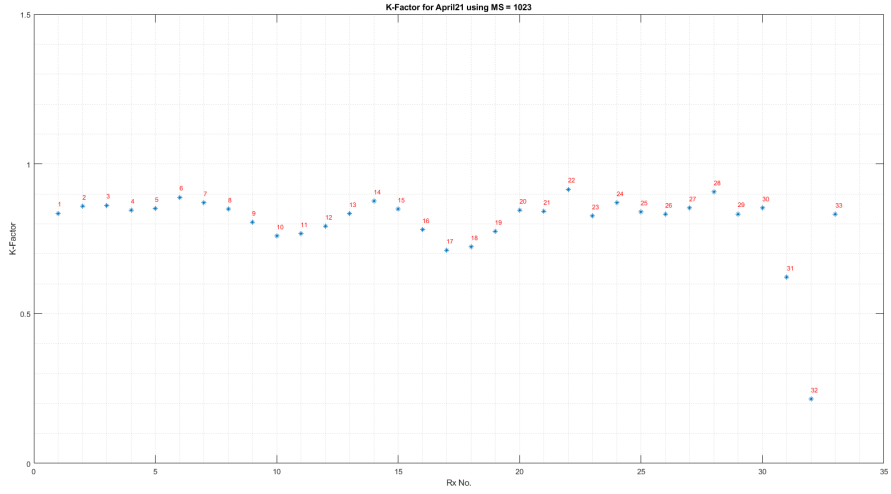

Figure 5.7.23: K-Factor of each Rx point.

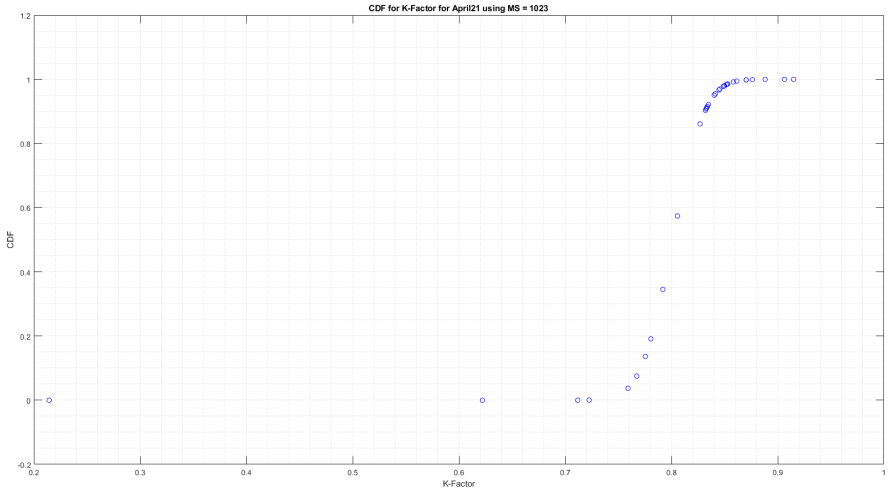

Figure 5.7.24: CDF and K-Factor.

Below is the table 5.1 for K-Factor values assigned to each Rx location in case of the 9.5 km field measurements:

Rx No.	K-Factor	Rx No.	K-Factor
1	0.83468050	17	0.71188068
2	0.85827088	18	0.72250611
3	0.86142230	19	0.77535194
4	0.84556442	20	0.84470165
5	0.85154098	21	0.84125519
6	0.88815379	22	0.91493410
7	0.87039316	23	0.82688147
8	0.84986043	24	0.87022030
9	0.80567414	25	0.84022331
10	0.75910693	26	0.83197153
11	0.76731086	27	0.85286450
12	0.79187268	28	0.90632004
13	0.83376014	29	0.83309418
14	0.87621433	30	0.85257965
15	0.84896737	31	0.62212026
16	0.78063869	32	0.21435717
		33	0.83262169

Table 5.1: K-Factor: For the vicinity of 9.5 Km Measurements

Moreover, the following table 5.2 is for the 5 km measurements field

As K-Factor is defined as the ratio between the variance of the multipath and the signal power, the value of K defines the fading distribution. For $K = 0$, which means that the dominant path is decreasing in amplitude, the Ricean distribution degenerates to a Rayleigh distribution [25]. It is observed that, K-Factor at the $9.5Km$ field is generally lower than the $5Km$ field measurements with a very small variation among the Rx points, while in far field more variation occurs. Generally, it is noticed that K values are > 0. Hence, we observe Ricean fading distribution, in which there is a dominant stationary signal component presents (LOS path).

Table 5.2: K-Factor Measurements: For distances less than 5 km

Rx No.	K-Factor	Rx No.	K-Factor	Rx No.	K-Factor	Rx No.	K-Factor	Rx No.	K-Factor
1	0.99868995	19	0.99434298	37	0.99108976	55	0.19516732	73	0.99322522
2	0.99886823	20	0.99777573	38	0.99483758	56	0.99299657	74	0.99794745
3	0.99865001	21	0.99894780	39	0.98779452	57	0.99764186	75	0.99866360
4	0.99912930	22	0.99835974	40	0.92571521	58	0.72234058		
5	0.99817264	23	0.99737459	41	0.80091250	59	0.30355299		
6	0.99875993	24	0.98967856	42	0.42200005	60	0.17875323		
7	0.99889725	25	0.99016458	43	0.44043198	61	0.99127901		
8	0.99914831	26	0.96082276	44	0.70889229	62	0.97913200		
9	0.99897277	27	0.99687034	45	0.17791690	63	0.57558662		
10	0.99824953	28	0.99522257	46	0.44484243	64	0.30543104		
11	0.99144804	29	0.87579322	47	0.98663104	65	0.29702985		
12	0.99424362	30	0.95501864	48	0.28109449	66	0.35053283		
13	0.99643618	31	0.99720103	49	0.65565312	67	0.99021244		
14	0.99831241	32	0.99405211	50	0.36709946	68	0.075345665		
15	0.99859947	33	0.99764925	51	0.38234282	69	0.99760848		
16	0.99790317	34	0.99734217	52	0.23140442	70	0.99858403		
17	0.99798101	35	0.98695743	53	0.93194854	71	0.99109280		
18	0.99794924	36	0.94507247	54	0.38852054	72	0.98831165		

5.7.6 Doppler Spread

As discussed in 5.5 , the Doppler spread is obtained by applying FFT to the CIRs. During Doppler measurements, we used a highway in Gebze, Kocaeli as our receiver locations by capturing data continuously at different locations along the road while the car was moving at almost a constant speed.

In order to obtain the power spectral density (PSD) for the received signal, we first extract the PSD for a fixed receiver location as in Fig. 5.7.25. We notice that there is a fixed offset which is 10 KHz added to the center frequency 86 MHz. The reason for that is, due to the carrier frequency of the single tone, at the receiver side, the carrier frequency is added to the center frequency.

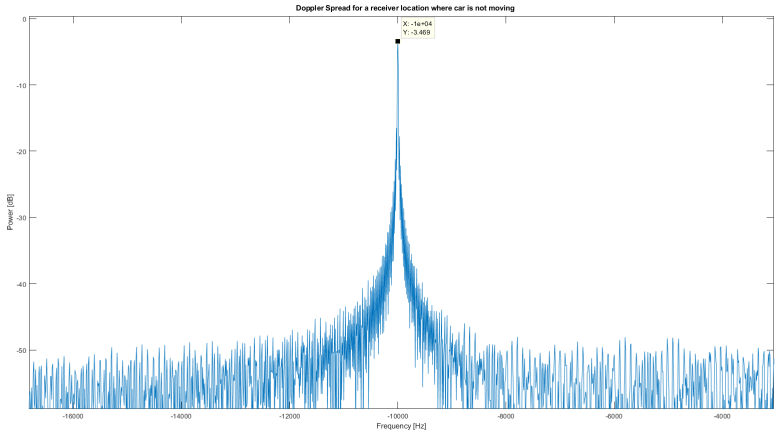

Figure 5.7.25: Doppler spread in a stationary receiver location.

On the other hand, for the non-stationary receiver locations points when the SUV was in the highway, all the result were similar to what is shown in Fig.5.7.26. We noticed the same Doppler shift as the stationary case in Fig. 5.7.25. The reason for this arises from the fact of the definition of the channel coherence time. The channel coherence time is an indication of the time varying nature of the channel. It is the time over which the CIR is invariant.The coherence time T_c is calculated as the inverse of the Doppler spread as $T_c = 0.423/f_m$, where f_m is the maximum Doppler shift given by $f_m = v/\lambda$ [25]. Since the Doppler shift

is very small, the channel coherence time T_c tends to be very large number. As a result, the coherence time of the FM channel is so large that the channel is almost invariant.

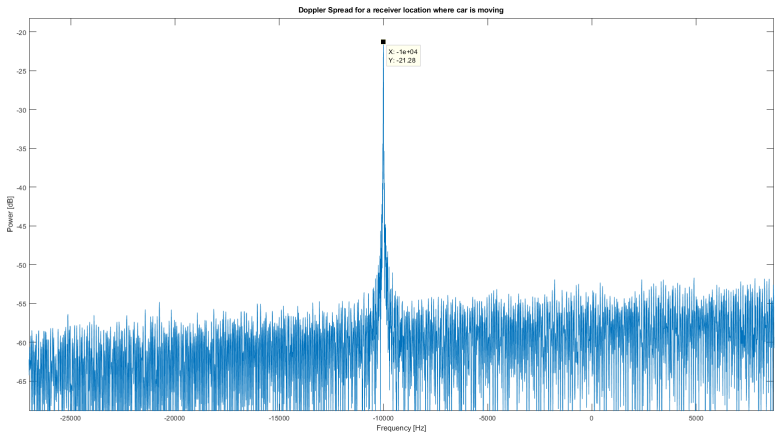

Figure 5.7.26: Doppler spread for a moving receiver location.

5.7.7 Path Loss

For the path loss, the reference point is determined to be 0.001 m, while the Tx power is set to be 44 dB. For the 5 km field shown in Fig. 4.4.1, the path loss and the received power for each receiver location are calculated. Moreover, the distances of the receiver locations are shown in Fig. 5.7.27.

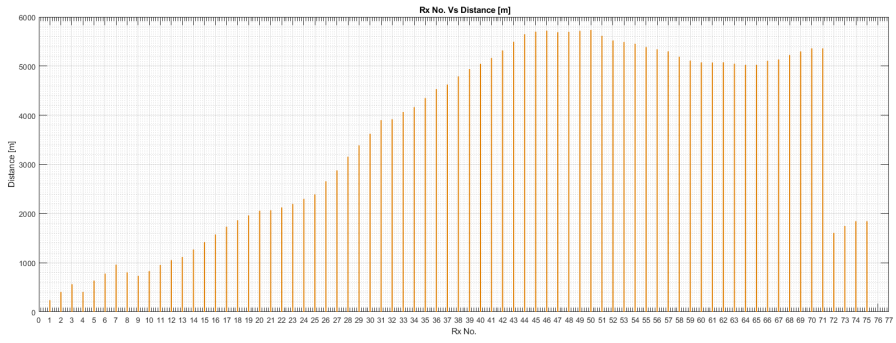

Figure 5.7.27: Distance of each receiver point for the site in Fig. 4.4.1.

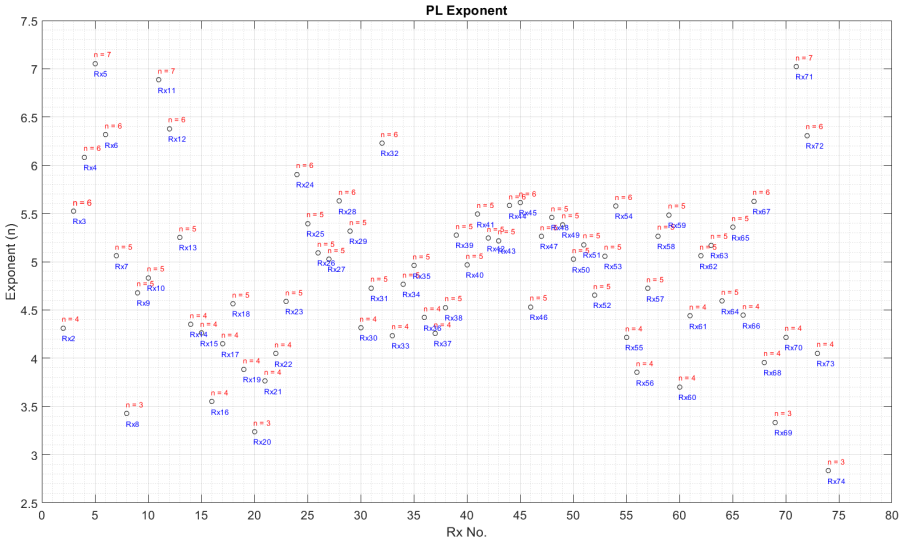

Figure 5.7.28: Path loss exponent for each receiver point for the site in Fig. 4.4.1.

Furthermore, the path loss exponent is shown in Fig. 5.7.28. Path loss exponent is the relation between the average received power and the distance. We notice that the path loss exponent is varying from 3 to 7 depends on the receiver location. Typically, for the free space $n = 2$, while for urban area $n = 2.7 - 3.5$. For suburban or badurban areas the PL exponent varies from $n = 3 - 6.5$ as discussed in [64, 65, 60]. We got $n = 8$ for only one receiver point for Rx 14 and we excluded it because it is irregular data that is the reason why there are only 74 Rx points in Fig 5.7.28.

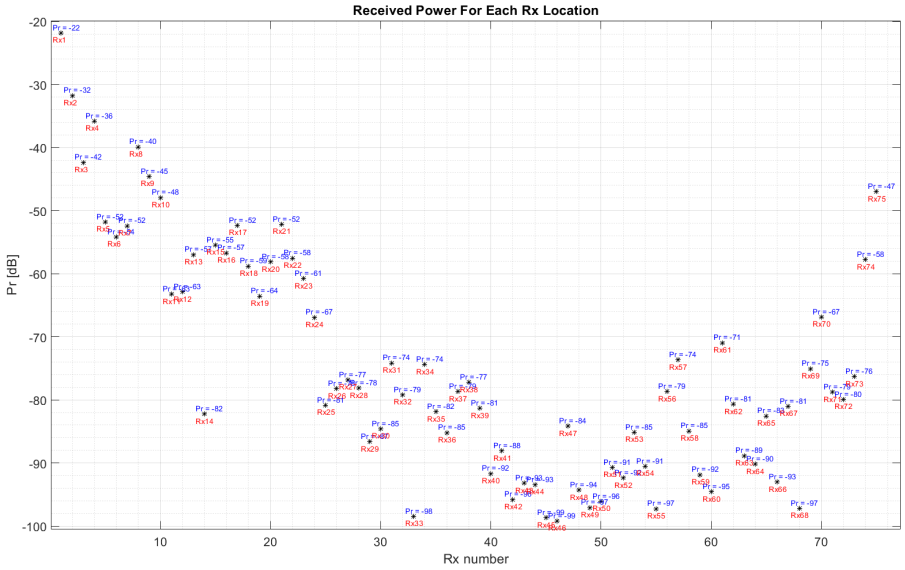

Figure 5.7.29: Received power for each receiver location for the site in Fig. 4.4.1.

Moreover, path loss calculations for the field measurements for the site in Fig. 4.4.1 are shown in Fig. 5.7.31. A gradual increase is observed as we move far from the transmitter location and vice versa. In general, for the theoretical path loss calculations that is shown in Fig. 5.7.30, we notice a similar trend to our measured path loss in Fig. 5.7.31.

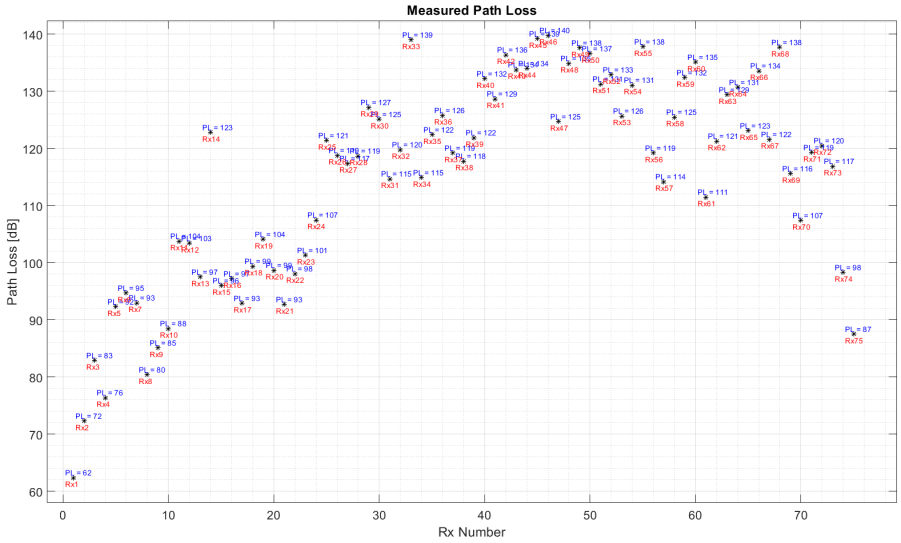

Figure 5.7.30: Measured Path Loss for each receiver location for the site in Fig. 4.4.1.

For the theoretical path loss, the values are smaller than the measured path loss from the field. On the other hand, for the received power in Fig. 5.7.29 we notice a general decay for the power as we go far from the transmitter and an arise as we move back near to the transmitter.

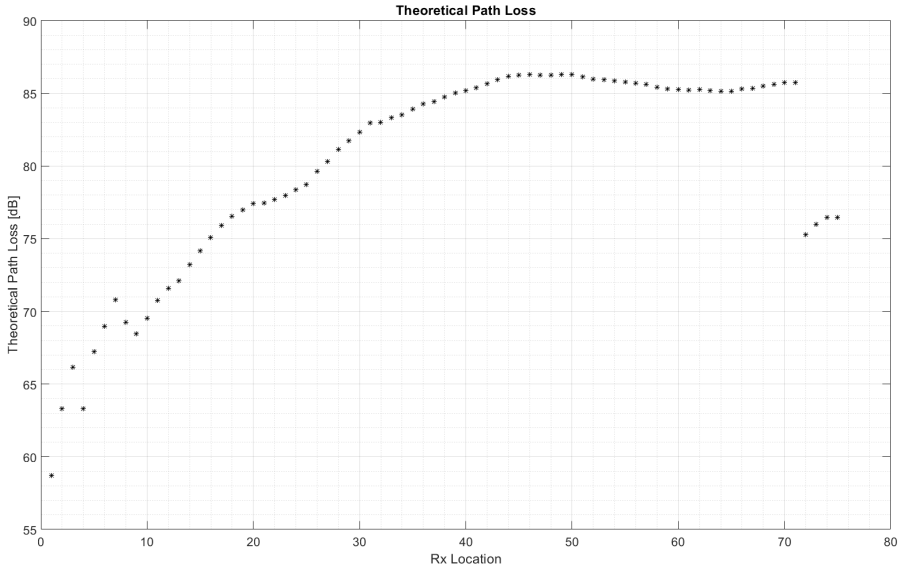

Figure 5.7.31: Theoretical Path Loss for each receiver location for the site in Fig. 4.4.1.

Despite of the near distance of some receiver locations to the transmitter, such as R_x3, R_x5, R_x6, the received power at a further distance locations, such asR_x8, R_x9, is better. The reason for that is the further distance receiver locations are lying into a region where there is a direct LOS with the transmitter, while the near distance receivers suffer from NLOS due to tall buildings and trees.

Chapter 6

Conclusion And Future Work

The process of understanding the behavior of a certain frequency band through actual measurements is an ideal approach to take, although it is a time-consuming and expensive process. Through field measurements the behavior of the channel should be accurately studied to be able to produce a final model that describe the channel dynamics precisely. Modelling the channel attributes is crucial in the analysis of many communication systems.

This thesis provided the results for outdoor measurements for the FM band channels, which to the best of the author's knowledge, is the first attempt towards utilizing and deeply understanding the behavior of such low frequency channels.

A measurement setup is developed in this study for both indoor and outdoor measurements. The proposed setup has many advantages. It can be used inside the car for the outdoor field. It is flexible and easy to implement. The setup takes around 15 minutes to be completely functional.

By using this setup we were able to measure data in different scenarios including urban areas and hilly terrain regions as shown in Figs. 4.4.1 and 4.4.2. The key channel parameters for the FM channel were obtained from the measured data, such as PDP, DoA, Doppler spread, K-Factor, and PL to fully understand the channel behaviour.

As for the PDPs, we notice as expected that we have usually in most of the cases strong LOS even for the far field measurements which is up to 9.5 Km. This is due to the durability of the FM signal due to the large wavelength. Large channel excess delay is noticed. In general excess delays beyond 20 μsec are observed, while channel coherence time is large which shows how the FM band channel does not change over a quite large time due to the low frequency propagation characteristics. We have observed that the FM channel possesses large delay spread especially in bad urban environments, making 4G and 5G's main waveform orthogonal frequency division multiplexing (OFDM) transmission less efficient.

For the direction of arrival, we notice a single angle for the LOS case while more than one angle in the NLOS case. Smoothing the covariance matrix is done to take the multipaths into account. A large angle spread is generally observed due to strong reflections around the receiver. As we observed signals coming from different angles, we suppose that MIMO in this band is possible.

A near to 1 Rician k-factor is observed along our measurements, which agrees with the LOS majority observed in the PDP results.

On the other hand, Doppler spread calculations and results are shown in this study for the FM band channel. Doppler spread is important to understand the effect of a moving receiver, and the small scale fading of the channel. As well as the coherence time which shows for how long the channel is nearly constant. We observed a very small Doppler shift that tends to zero, as there is no change in the Doppler shift when the SUV was stationary and during its movement. Hence, the coherence time is so large. Thus, the FM band channel is time invariant.

Furthermore, Path loss is extremely important to any wireless system as it determines many components of the system such as the transmitted power, the antenna gains, and locations. In this thesis it is shown the results for the path loss for both a less than 5 Km field and less than 9.5 Km field measurements. Path loss exponent is also obtained for each receiver location and observed to be in the range of $3 - 7$.

Almost the key channel characteristics for our measurements for the FM band channel has been obtained and provided in this study. Additionally, as mentioned in 1, low frequencies are grasping researchers' attention. An example for that is the TV white space. Moreover, since the FM band usage is degrading with time due to using the internet as an alternative, this band can be greatly used in different important applications.

Generally, the band has good penetration through different environments, and hence, with new waveform design in 5G, like non-orthogonal multiple access (NOMA), it can be utilized for supplementary downlink channel, instead of being under-utilized for analog FM music broadcast. Moreover, with 5G systems also targeting vehicle-to-vehicle communication, since the band has large channel coherence time, it stands as a strong candidate to be used as the frequency band of vehicle-to-vehicle communication as well as infrastructure networks, and new digital audio broadcast services.

Bibliography

[1] "Guglielmo marconi." http://iwcmediaecology.pbworks.com/w/page/8480806/GuglielmoMarconi. Accessed: 2018-07-1.

[2] "Communication dsp algorithms and integrated circuits: Mimo preprocessing and detection processors." http://www.ee.nthu.edu.tw/~yhhuang/CommunicationDSPAlgorithmandIC.html. Accessed: 2018-07-1.

[3] Hindawi, "An example of a measured delay power profile, showing distinct clusters.." http://www.hindawi.com/journals/ijap/2010/735434/fig7/.

[4] Z.Pedrini, "What is isi (inter symbol interference) in lte?." http://www.telecomhall.com/what-is-isi-inter-symbol-interference-in-lte.aspx. Accessed: 2018-07-1.

[5] C.Chen, "The universe's doppler effect." http://princetoninnovation.org/magazine/2015/12/09/redshift-universes-doppler-effect/. Accessed: 2018-07-1.

[6] http://www.cntr.salford.ac.uk/comms/ebirth.php.

[7] http://www.telcomhistory.org/vm/histories.shtml.

[8] C. Doubts, "What is 1g or first generation of wireless telecommunication technology?." http://www.cleardoubts.com/technology/what-is-1g-or-first-generation-of-wireless-telecommunication-technology/. Accessed: 2018-07-1.

[9] "1g, 2g, 3g, 4g, 4g lte, 5g - what are these new technologies anyway?." https://whatsag.com/. Accessed: 2018-07-1.

[10] "Get ready for 5g." https://networks.nokia.com/5g/get-ready. Accessed: 2018-07-1.

[11] G. Foschini and M. Gans, "On limits of wireless communications in a fading environment when using multiple antennas," *Wireless personal communications*, vol. 6, no. 3, pp. 311–335, 1998.

[12] "Federal Communications Commission." http://www.fcc.gov/. Accessed: 2018-07-1.

[13] E. Woyke, "World's First Commercial White Spaces Network Launching Today In North Carolina." https://www.forbes.com/sites/elizabethwoyke/2012/01/26/worlds-first-commercial-white-spaces-network-launching-today-in-north-caroli Mar 2012.

[14] "Agility white space radio (AWR)." http://ktswireless.com/agility-white-space-radio-awr/.

[15] Dante, "FCC approves first white space device and spectrum database." https://www.theverge.com/2011/12/22/2656177/fcc-approves-first-white-space-spectrum-device-database, Dec 2011.

[16] A. A. Hassan, D. A. Reed, P. W. Garnett, and B. Anders, "White space utilization," Jun 2012.

[17] A. B. Flores, R. E. Guerra, E. W. Knightly, P. Ecclesine, and S. Pandey, "IEEE 802.11af: a standard for TV white space spectrum sharing," *IEEE Communications Magazine*, vol. 51, no. 10, p. 92?100, 2013.

[18] L. Indvik, "Study: More young adults tuning out terrestrial radio while driving." http://mashable.com/2013/04/02/internet-radio-study-npd/, Apr 2013.

[19] "Half of uk listens to online radio." http://advanced-television.com/2013/06/12/half-of-uk-listens-to-online-radio/.

[20] "Revenue - online radio 2003-2013 | forecast." https://www.statista.com/statistics/265681/online-radio-revenue-worldwide/.

[21] A. Saleh and R. Valenzuela, "A Statistical Model for Indoor Multipath Propagation," *Selected Areas in Communications, IEEE Journal on*, vol. 5, pp. 128–137, February 1987.

[22] A. Hossam, "A 140 mhz hardware channel emulator and fm directional wireless channel model for an outdoor environment," Master's thesis, Istanbul Sehir University, Istanbul, Turkey, 2016.

[23] H. Asplund, A. Glazunov, A. Molisch, K. Pedersen, and M. Steinbauer, "The COST 259 Directional Channel Model - Part II: Macrocells," *Wireless Communications, IEEE Transactions on*, vol. 5, pp. 3434–3450, December 2006.

[24] M. Zhu, G. Eriksson, and F. Tufvesson, "The COST 2100 channel model: Parameterization and validation based on outdoor MIMO measurements at 300 MHz," *Wireless Communications, IEEE Transactions on*, vol. 12, no. 2, pp. 888–897, 2013.

[25] T. S. Rappaport *et al.*, *Wireless communications: principles and practice*, vol. 2. prentice hall PTR New Jersey, 1996.

[26] A. F. Molisch, *Wireless communications*. Wiley-Blackwell, 2010.

[27] D. Tse and P. Viswanath, *Fundamentals of wireless communication*. Cambridge University Press, 2008.

[28] R. Sevlian, C. Chun, I. Tan, A. Bahai, and K. Laberteaux, "Channel characterization for 700 mhz dsrc vehicular communication," *Journal of Electrical and Computer Engineering*, vol. 2010, pp. 1–9, 2010.

[29] D. Cox, "Delay doppler characteristics of multipath propagation at 910 mhz in a suburban mobile radio environment," *IEEE Transactions on Antennas and Propagation*, vol. 20, pp. 625–635, September 1972.

[30] A. F. Molisch, H. Asplund, R. Heddergott, M. Steinbauer, and T. Zwick, "The cost259 directional channel model-part i: Overview and methodology," *IEEE Transactions on Wireless Communications*, vol. 5, pp. 3421–3433, December 2006.

[31] P. Pathania, P. Kumar, and S. Rana, "A modified formulation of path loss models for broadcasting applications," *International Journal of Recent Technology and Engineering (IJRTE)*, pp. 2277–3878, 08 2014.

[32] M. Meeks, "Vhf propagation over hilly, forested terrain," *IEEE Transactions on Antennas and Propagation*, vol. 31, pp. 483–489, May 1983.

[33] A. Aitelieva and G. Ã. v. H. ÃĞelebi, "Ray tracing-based channel modelling for vhf frequency band," in *2015 23nd Signal Processing and Communications Applications Conference (SIU)*, pp. 1385–1388, May 2015.

[34] A.Aitalieva, "VHF Channel Modeling for Wireless Sensor Networks," Master's thesis, Gebze Technical University, Gebze, Kocaeli, Turkey, 2015.

[35] A. Zogg, "Multipath delay spread in a hilly region at 210 mhz," *IEEE Transactions on Vehicular Technology*, vol. 36, pp. 184–187, Nov 1987.

[36] T. S. Rappaport, S. Y. Seidel, and R. Singh, "900-mhz multipath propagation measurements for us digital cellular radiotelephone," *IEEE Transactions on Vehicular Technology*, vol. 39, pp. 132–139, May 1990.

[37] R. Nilsson and J. van de Beek, "Channel measurements in an open-pit mine using usrps: 5g; expect the unexpected," in *2016 IEEE Wireless Communications and Networking Conference*, pp. 1–6, April 2016.

[38] T. S. Rappaport, J. H. Reed, and B. D. Woerner, "Position location using wireless communications on highways of the future," *IEEE Communications Magazine*, vol. 34, pp. 33–41, Oct 1996.

[39] U. Sarac, F. K. Harmanci, and T. Akgul, "Experimental analysis of detection and localization of multiple emitters in multipath environments," *IEEE Antennas and Propagation Magazine*, vol. 50, pp. 61–70, Oct 2008.

[40] R. Schmidt and R. Franks, "Multiple source df signal processing: An experimental system," *IEEE Transactions on Antennas and Propagation*, vol. 34, pp. 281–290, March 1986.

[41] L. C. Godara, "Application of antenna arrays to mobile communications. ii. beam-forming and direction-of-arrival considerations," *Proceedings of the IEEE*, vol. 85, pp. 1195–1245, Aug 1997.

[42] K. Kalliola, H. Laitinen, L. I. Vaskelainen, and P. Vainikainen, "Real-time 3-d spatial-temporal dual-polarized measurement of wideband radio channel at mobile station," *IEEE Transactions on Instrumentation and Measurement*, vol. 49, pp. 439–448, Apr 2000.

[43] M.-S. Lee, V. Katkovnik, and Y.-H. Kim, "System modeling and signal processing for a switch antenna array radar," *IEEE Transactions on Signal Processing*, vol. 52, pp. 1513–1523, June 2004.

[44] H. Xin and J. Ding, "An improved two-antenna direction of arrival (doa) technique inspired by human ears," in *2008 IEEE Antennas and Propagation Society International Symposium*, pp. 1–4, July 2008.

[45] A. Gorcin and H. Arslan, "A two-antenna single rf front-end doa estimation system for wireless communications signals," *IEEE Transactions on Antennas and Propagation*, vol. 62, pp. 5321–5333, Oct 2014.

[46] B. H. Wang, H. T. Hui, and M. S. Leong, "Decoupled 2d direction of arrival estimation using compact uniform circular arrays in the presence of elevation-dependent mutual coupling," *IEEE Transactions on Antennas and Propagation*, vol. 58, pp. 747–755, March 2010.

[47] Z. Ye and C. Liu, "On the resiliency of music direction finding against antenna sensor coupling," *IEEE Transactions on Antennas and Propagation*, vol. 56, pp. 371–380, Feb 2008.

[48] S. Preston, D. Thiel, T. Smith, S. Okeefe, and J. W. Lu, "Base-station tracking in mobile communications using a switched parasitic antenna array," *IEEE Transactions on Antennas and Propagation*, vol. 46, no. 6, p. 841âĂŞ844, 1998.

[49] T. Svantesson and M. Wennstrom, "High-resolution direction finding using a switched parasitic antenna," in *Statistical Signal Processing, 2001. Proceedings of the 11th IEEE Signal Processing Workshop on*, pp. 508–511, IEEE, 2001.

[50] A. Hirata, E. Taillefer, H. Yamada, and T. Ohira, "Handheld direction of arrival finder with electronically steerable parasitic array radiator using the reactance-domain multiple signal classification algorithm," *IET Microwaves, Antennas and Propagation*, vol. 1, no. 4, p. 815, 2007.

[51] R. Degroat, E. Dowling, and D. Linebarger, "The constrained MUSIC problem," *IEEE Transactions on Signal Processing*, vol. 41, no. 3, p. 1445âĂŞ1449, 1993.

[52] B. Porat and B. Friedlander, "Analysis of the asymptotic relative efficiency of the music algorithm," *IEEE Transactions on Acoustics, Speech, and Signal Processing*, vol. 36, pp. 532–544, April 1988.

[53] G. Byun, H. Choo, and H. Ling, "Optimum placement of df antenna elements for accurate doa estimation in a harsh platform environment," *IEEE Transactions on Antennas and Propagation*, vol. 61, pp. 4783–4791, Sept 2013.

[54] K. R. Srinivas and V. U. Reddy, "Finite data performance of music and minimum norm methods," *IEEE Transactions on Aerospace and Electronic Systems*, vol. 30, pp. 161–174, Jan 1994.

[55] S. Pillai and B. Kwon, "Forward/backward spatial smoothing techniques for coherent signal identification," *IEEE Transactions on Acoustics, Speech, and Signal Processing*, vol. 37, no. 1, p. 8âĂŞ15, 1989.

[56] C. Tepedelenlioglu, A. Abdi, and G. B. Giannakis, "The ricean k factor: estimation and performance analysis," *IEEE Transactions on Wireless Communications*, vol. 2, pp. 799–810, July 2003.

[57] T. Zhou, C. Tao, L. Liu, and Z. Tan, "Ricean k-factor measurements and analysis for wideband radio channels in high-speed railway u-shape cutting scenarios," in *2014 IEEE 79th Vehicular Technology Conference (VTC Spring)*, pp. 1–5, May 2014.

[58] I. Tan, W. Tang, K. Laberteaux, and A. Bahai, "Measurement and analysis of wireless channel impairments in dsrc vehicular communications," in *2008 IEEE International Conference on Communications*, pp. 4882–4888, May 2008.

[59] S. Guzelgoz, S. Yarkan, and H. Arslan, "Investigation of time selectivity of wireless channels through the use of rvc," *Measurement*, vol. 43, no. 10, pp. 1532 – 1541, 2010.

[60] V. S. Abhayawardhana, I. J. Wassell, D. Crosby, M. P. Sellars, and M. G. Brown, "Comparison of empirical propagation path loss models for fixed wireless access systems," in *2005 IEEE 61st Vehicular Technology Conference*, vol. 1, pp. 73–77 Vol. 1, May 2005.

[61] H. Asplund, A. A. Glazunov, A. F. Molisch, K. I. Pedersen, and M. Steinbauer, "The cost 259 directional channel model-part ii: macrocells," *IEEE Transactions on Wireless Communications*, vol. 5, no. 12, 2006.

[62] A. H. Mohammed and M. K. Ozdemir, "A directional FM channel model for contemporary wireless systems," *Canadian Journal of Electrical and Computer Engineering*, vol. 39, no. 4, pp. 311–321, 2016.

[63] C. of the European Communities, *Digital Land Mobile Radio Communications - COST 207: Final Report*. Official Publications of the European Communities, 1989.

[64] I. R. Sector, "Guidelines for evaluation of radio transmission technology for imt-2000," *Recommendation ITU-R M*, vol. 1225, 1997.

[65] A. Goldsmith, *Wireless Communications*. New York, NY, USA: Cambridge University Press, 2005.

FM BAND CHANNEL MEASUREMENTS AND MODELLING

ORIGINALITY REPORT

11%	8%	8%	2%
SIMILARITY INDEX	INTERNET SOURCES	PUBLICATIONS	STUDENT PAPERS

MATCH ALL SOURCES (ONLY SELECTED SOURCE PRINTED)

1%

★ core.ac.uk

Internet Source

Exclude quotes	Off	Exclude matches	Off
Exclude bibliography	On		